Tolerance Analysis of Flexible Assemblies Using Finite Element and Spectral Analysis

ADCATS Report No. 99-1

Bryan F. Bihlmaier, graduate student
Department of Mechanical Engineering
Brigham Young University

MS thesis sponsored by ADCATS

April 1999

ABSTRACT

Traditional tolerance analysis assumes rigid parts. Traditional methods can not account for deformations or stresses due to assembly. Rigid body tolerance analysis over-estimates variations in flexible assemblies, because flexible parts deform under assembly loads to compensate for manufacturing variations. This paper proposes a new method for modeling flexible assemblies, called the Flexible Assembly Spectral Tolerance Analysis (FASTA) method, which uses the autocorrelation function from frequency spectrum analysis to model random surface variations.

Finite element models are used to predict assembly forces and stresses from known surface variations. Variations at surface nodes are not independent variables. Therefore, covariance must be included in the statistical analysis of flexible assemblies. Covariance between nodes arises from both material elastic coupling and surface continuity constraints. This paper shows how covariance is included in statistical predictions, and how to calculate the covariance matrix from autocorrelation functions of part surfaces. Deterministic variations, such as part warping, are separated from random variations.

The proposed method agrees well with Monte Carlo simulations, but requires much shorter computation times. The FASTA method is most useful as a design and tolerance allocation tool. The expected range of stresses and deformations from assembly processes may be statistically predicted before parts are manufactured, based on surface tolerances.

TABLE OF CONTENTS

LIST OF FIGURES

LIST OF TABLES

Chapter 1

INTRODUCTION

Tolerance analysis predicts the effect that variations in manufactured parts will have on an assembly. Manufactured parts naturally deviate from the nominal geometry, usually within a specified tolerance zone. Tolerance analysis can be used to economically allocate part tolerances to those features which affect the overall function or assemblability of an assembly. Part variations which affect assemblies are size, form, surface, and kinematic variations. Size variations are deviations from nominal dimensions such as length and diameter. Form variations vary from the nominal shape, such as out-of-round holes. Surface variations are small irregularities in surfaces due to the manufacturing process. Kinematic variations occur during assembly when parts adjust their positions slightly due to gaps or interferences between mating parts.

The analysis of assembly variations generally assumes rigid parts. It does not account for deformations of individual parts during assembly. Rigid body analysis tends to over-estimate assembly variation in an assembly of flexible components and cannot predict resulting stresses and deformations. Thin and easily deformable parts, such as sheet metal or composite laminates, cannot be accurately modeled using these methods. A separate method is needed to analyze assemblies of flexible or compliant parts.

Sheet metal and composite laminate parts are used often in the aerospace, automotive, and many other areas. For example, the skin of an aircraft wing typically is assembled from many smaller sheets of pre-formed sheet metal riveted together. Variations in the sheet metal parts result in residual assembly stresses which could cause the wing to fail prematurely. Also, shape deformations due to assembly could affect the aerodynamic properties of the wing. Automotive bodies are another common example of flexible assemblies. Aesthetics, among other considerations, could be affected by deformations due to part variation. Vibrational noise is also affected by assembly stresses. A method for accurately modeling assemblies of compliant parts is clearly needed in these areas.

The problem in tolerance analysis of flexible assemblies is how to statistically represent a population of surface variations, and how this representation can be used to predict the probable range of assembly forces and distortions. Also, how to separate deterministic (non-random) variations, such as part warping, from those variations due to random sources of error.

This paper presents a new method for modeling assemblies of flexible parts by representing surface variations using Fourier, or frequency spectrum, analysis. A frequency spectrum model can be used to represent any part shape, including both nominal and variational shapes. From frequency spectrum models, statistical information can be obtained which may be used as input into a finite element model of the parts. The finite element model can then be used to predict the probable range of forces, stresses,

and part deformations due to assembly. The proposed method is called the Flexible Assembly Spectral Tolerance Analysis method, or FASTA.

The remainder of this paper describes and verifies a method for using spectral analysis to statistically analyze assemblies of flexible parts. Chapter 2 presents a brief review of research related to the area of flexible assembly tolerance analysis. A review of previous work on statistical force and deformation solutions to finite element models of flexible assemblies is presented in Chapter 3. Chapter 4 describes basic concepts of spectral analysis and their application in forming statistical covariance matrices, and explains the necessary assumptions. Statistical force results from several independent methods are compared in Chapter 5 to verify the new spectral analysis method. In Chapter 6, a new method is outlined for statistically predicting residual stresses throughout each part in a flexible assembly. Chapter 7 includes a verification study of statistical stress results. The effect of different wavelengths of surface variation on the resulting stresses in a flexible assembly is investigated in Chapter 8. Chapter 9 discusses several important issues related to the measurement and design of part surfaces using spectral analysis. Conclusions, significant contributions, and recommendations for future work are summarized in Chapter 10.

Chapter 2

BACKGROUND LITERATURE REVIEW

Little work has been done in the area of flexible assembly tolerance analysis. Some of the first research related to this area was done by Gordis and Flannely (1994). They used frequency domain structural analysis to predict in-plane loads and displacements from misalignment of fastener holes in flexible components.

A leading researcher in the area of flexible assembly tolerance analysis is Hu of the University of Michigan. He has used simple finite element models to predict assembly variation of flexible sheet metal assemblies (Liu 1995, 1997). His work has focused on the effect of part fixturing and order of assembly. He has not investigated the effect of surface variations on flexible assemblies, and therefore has not included covariance between finite element nodes in his analyses.

Merkley (1998) recently proposed a new method for tolerance analysis of flexible assemblies. He uses the assumptions of Francavilla and Zienkiewicz (1975) to linearize the elastic contact problem between mating flexible parts. Merkley derived a method for predicting the mean and variance of assembly forces and deformations due to assembling two flexible parts having surface variations. He describes the need for a covariance matrix representing the interrelation of variations at neighboring nodes in the finite

element model. The interrelation is due to both surface continuity, which he calls geometric covariance, and elastic coupling, which he calls material covariance. Merkley used random Bezier curves to describe surface variations and to calculate geometric covariance. He also showed that material covariance effects are described by the finite element stiffness matrix. Stout (unpublished) followed Merkley-s work by using polynomial curve fits to produce the geometric covariance matrix. Merkley described surface variation in terms of a tolerance band specified about the nominal surface. Stout investigated the effect of different wavelength surface variations on assembly results. This paper builds on Merkley and Stout-s work, presenting a new method for deriving the covariance matrix using spectral analysis techniques. The new method, called the Flexible Assembly Spectral Tolerance Analysis method, or FASTA, also includes the effect of surface variation wavelength on assemblies.

Chapter 3

STATISTICAL TOLERANCE ANALYSIS USING FINITE ELEMENT ANALYSIS

Tolerance analysis of flexible parts requires a model for calculating part deformations, as well as forces and internal stresses due to assembly. To predict such assembly results, the parts may be modeled using a finite element model. In the finite element model, specified nodes along the contacting surfaces represent fasteners. Statistical boundary conditions are placed on the mating surface nodes, representing the vector of gaps between aligning nodes of the two parts. The gap vector is the difference between the surface variation of the two parts. When assembled, the parts are assumed to be deformed by closure forces from each fastener such that the parts are contacting, or the gap vector is zero, at every fastener node along the mating surfaces.

In a statistical analysis, the boundary conditions applied to the finite element model are random variables due to surface variations, rather than constant known values. Statistical analyses of finite element models require a covariance matrix describing the interrelation of nodal displacements along contacting surfaces. Merkley was the first to recognize the need for including covariance in statistical finite element analyses when using random variables as input.

3.1 Assumptions

The finite element solution presented by Francavilla and Zienkiewicz (1975) for elastic contact problems is applicable to flexible assemblies subject to closure forces. Their method requires several assumptions which limits its use, but are well-suited to the analysis of flexible assemblies. The method requires that contact be enforced at each node in the contact zone, and that the boundaries of the contact zone be known beforehand. In the flexible assembly problem, the parts are to be assembled along specified mating surfaces, so the contact region is well-defined.

To model a flexible assembly, specified boundary nodes along mating surfaces are modeled as fasteners. For exact solutions, contact is enforced at fastener nodes and other nodes are left unconstrained. The assembled parts must be checked for interference at nodes between fasteners. If there is interference, the gap at interfering nodes is constrained to be zero, and another solution must be performed. This process is repeated until there is no interference along the mating surfaces. If the surface variations are small and the fasteners are spaced sufficiently close together, there will be very little interference when the gap is initially forced to close at fastener nodes. Reasonably accurate results may be obtained, therefore, by ignoring possible interference between fasteners and performing one solution which forces contact at all fastener nodes along the mating surfaces. The iterative method required for an exact solution is avoided, making the finite element assembly model linear. This linear finite element assembly model is used in the FASTA method.

3.2 Stiffness Matrix Condensation

Finite element stiffness matrices are generally very large and sparsely populated. In the assembly of flexible parts, only boundary nodes along fixed and mating edges need to be involved in the analysis. To reduce computation time, the stiffness matrices for the two parts can be reduced to stiffness matrices containing terms relating only to the boundary node degrees of freedom, while still retaining the influence of the interior nodes. This process is called matrix condensation, and the resulting stiffness matrix represents what is often called a super-element. Reduced stiffness matrices are ideally suited to assembly problems (Merkley 1996). Each part may be represented as a single super-element. Tolerance analysis may then be performed on a greatly reduced assembly model.

To reduce a stiffness matrix, the finite element stiffness equation

$$\{F\} = [K]\{\delta\} \tag{3.1}$$

is partitioned into elements K_{bb} relating boundary nodal displacements $ä_b$ to boundary nodal forces F_b, elements K_{ii} relating internal nodal displacements $ä_i$ to internal forces F_i, and elements K_{bi} and K_{ib} relating boundary and internal displacements and forces. The displacement and force vectors are similarly partitioned, as shown below.

$$\begin{Bmatrix} F_b \\ \hdashline F_i \end{Bmatrix} = \left[\begin{array}{c:c} K_{bb} & K_{bi} \\ \hdashline K_{ib} & K_{ii} \end{array}\right] \begin{Bmatrix} \delta_b \\ \hdashline \delta_i \end{Bmatrix} \tag{3.2}$$

Because there are no forces applied to interior nodes, this equation can be rewritten as

$$\{F_b\} = [K_{bb}]\{\delta_b\} + [K_{bi}]\{\delta_i\} \tag{3.3}$$

and

$$\{F_i\} = [K_{ib}]\{\delta_b\} + [K_{ii}]\{\delta_i\} = \{0\} . \tag{3.4}$$

Equation 3.4 can be solved for $\ddot{a}_i$:

$$\{\delta_i\} = -[K_{ii}^{-1}][K_{ib}]\{\delta_b\}.$$

This result can be substituted into Equation 3.3, giving:

$$\begin{aligned}\{F_b\} &= [K_{bb}]\{\delta_b\} - [K_{bi}][K_{ii}^{-1}][K_{ib}]\{\delta_b\} \\ &= \left([K_{bb}] - [K_{bi}][K_{ii}^{-1}][K_{ib}]\right)\{\delta_b\}. \end{aligned} \quad (3.5)$$

Comparing Equation 3.5 to the stiffness equation 3.1, it can be seen that the reduced stiffness matrix, K_r, is:

$$[K_r] = [K_{bb}] - [K_{bi}][K_{ii}^{-1}][K_{ib}]. \quad (3.6)$$

The reduced stiffness matrix only contains terms involving the boundary degrees of freedom, but retains the influence of all interior nodes. For moderately large parts, the reduction in size of the stiffness matrix is quite significant and the extra computation time required to evaluate it is saved when performing further finite element calculations. If stresses or displacements at interior points are desired, a subsequent analysis is required in which the original, unreduced stiffness matrices must be used, along with appropriate boundary conditions, to solve for internal values.

3.3 Equivalent Stiffness Matrix

The force required to close the gap between two mating part surfaces may be expressed in terms of an equivalent stiffness matrix K_{eq}, relating the closure force to the total gap between the surfaces. This can further simplify the finite element assembly model by combining the stiffness matrices of two mating parts into one equivalent stiffness

matrix. An example of two springs in series will illustrate this technique.

Suppose two linear springs with stiffness K_A and K_B, separated by a gap $ä_0$, are connected in series as shown in Figure 3.1.

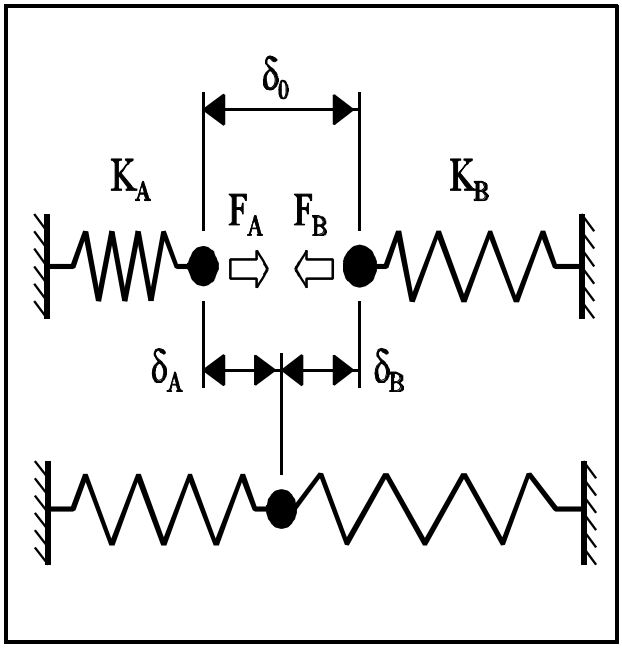

Figure 3.1 Two linear springs assembled in series.

At equilibrium, the force on each spring will be equal, and the total deflection will be the sum of the deflection of the two springs:

$$\delta_0 = \delta_A + \delta_B . \tag{3.7}$$

By solving the stiffness equation for each spring, the force equilibrium equation, and the gap equation 3.7 simultaneously, the equivalent stiffness of the two springs in series can be found:

$$K_{eq} = \frac{F}{\delta_0} = \frac{1}{\frac{1}{K_A} + \frac{1}{K_B}} = \frac{K_A K_B}{K_A + K_B} \tag{3.8}$$

Also, the ratio between the deflection of each spring and the total gap between the springs can be described by the stiffness ratio of each spring, K_{rA} and K_{rB}:

$$\delta_A = \frac{K_B}{K_A + K_B}\delta_0 = K_{rA}\delta_0 \tag{3.9}$$

and

$$\delta_B = \frac{K_A}{K_A + K_B}\delta_0 = K_{rB}\delta_0 \tag{3.10}$$

These results may be rewritten for two linearly-elastic parts assembled by closure forces acting on the mating surfaces. If the two parts are represented by a finite element model, the vector of closure forces along the mating surfaces, F, can be expressed in terms of an equivalent stiffness matrix, K_{eq}, and the total gap vector between mating surface nodes, $ä_0$:

$$\{F\} = \left[K_{eq}\right]\{\delta_0\}.$$

Similar to Equation 3.8, the equivalent super-element stiffness matrix, relating the vector of closure forces to the vector of gaps between mating nodes, is

$$\begin{aligned}\left[K_{eq}\right] &= \left[K_A\right]\left[K_A + K_B\right]^{-1}\left[K_B\right] \\ &= \left[K_B\right]\left[K_A + K_B\right]^{-1}\left[K_A\right],\end{aligned} \tag{3.11}$$

where K_A and K_B are the super-element stiffness matrices of the two parts. Equations 3.9 and 3.10 can also be written in matrix form, relating the vector of nodal displacements along the mating surface of each part, $ä_A$ or $ä_B$, to the total gap vector $ä_0$:

$$\{\delta_A\} = [K_A + K_B]^{-1}[K_B]\{\delta_0\} = [K_{rA}]\{\delta_0\} \tag{3.12}$$

and

$$\{\delta_B\} = [K_A + K_B]^{-1}[K_A]\{\delta_0\} = [K_{rB}]\{\delta_0\}. \tag{3.13}$$

The stiffness ratios can be used to find the boundary displacement vector for each part, given the gap vector between parts. In the special case of joining two identical parts, these ratios are simply ½ for each part. The mating edge of each part deflects one-half of the distance between the two mating edges. Using an equivalent stiffness matrix and stiffness ratios, the finite element model for an assembly can be simplified if all that is needed are the closure forces along boundary nodes and deflections of boundary nodes for each part.

3.4 Example Statistical Solution

To demonstrate performing statistical tolerance analysis on finite element models, a sample problem will be presented and solved using statistical methods. The problem is a simple assembly of two identical flat plates which are fastened along a common mating edge, as in Figure 3.2. Each part measures 10 by 10 inches and is 0.10 inches thick. The plates are made from a material with modulus of elasticity 10×10^6 psi and Poisson's ratio 0.30.

There are variations along the mating edge of each part which cause a gap between the parts. The surface variation for a population of these parts, measured perpendicular to the plates, has mean 0 and standard deviation 0.0236 inches everywhere along the mating

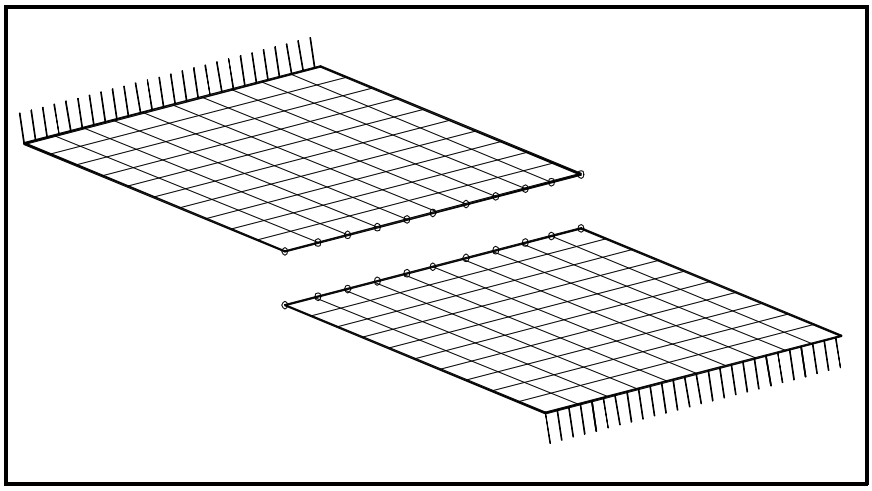

Figure 3.2 Lap joint finite element model.

edge. The mean of the gap is the sum of the mean of each surface. And, because the surface variations of each part are independent, the variance of the gap is the sum of the variance of the two part surfaces. Therefore, the gap has mean $\mu_0 = 0$ and standard deviation $ó_0 = 0.0333$ inches.

Initially, both parts were meshed into a 10 by 10 grid of 100 bending-only, 4-node plate elements. Each node of the plate elements has three degrees of freedom: one out-of-plane translation and two edge rotations. Every node along the mating edges was considered a fastener. The 11 fastener nodes were forced together in translation when assembled, but the rotations were not constrained. The individual stiffness matrices were calculated and condensed into super-elements involving only boundary nodes along the mating and fixed edges. The boundary nodes where the super-elements are to be fastened together are circled in Figure 3.2. With closure forces only applied in one degree of freedom per node along the mating edge, and three constrained degrees of freedom per node along the fixed edge, the super-element stiffness matrix had 44 degrees of freedom.

In this example, only the forces applied along the mating edge were of interest, and the displacements along the fixed edge were zero. Therefore, the super-element stiffness equation was partitioned and solved for only the mating-edge degrees of freedom. The problem was further simplified by forming one equivalent stiffness matrix for both parts. Because the two parts are identical, the stiffness ratio for both parts is ½ The resulting equivalent super-element stiffness matrix equation had only 11 degrees of freedom, compared to 726 degrees of freedom if the full system were solved.

To predict the distribution of closure forces, two solutions were required, one to find the mean closure force vector, and one to find the variance and standard deviation of the closure forces. In this case, the mean gap vector was {0}, and therefore the mean closure force vector was also {0}. Because the standard deviation of the surface variations was assumed to be uniform along the mating edges, the standard deviation gap vector, ó$_0$, was also uniform:

$$\{\sigma_0\} = 0.0333\begin{bmatrix}1 & 1 & 1 & 1 & 1 & 1 & 1 & 1 & 1 & 1 & 1\end{bmatrix}^T.$$

If nodal displacements along the mating edge are assumed to be independent, the terms in the closure force variance vector, σ_F^2, are found from

$$\sigma_F^2(i) = \sum_{j=1}^{dof} \left(K_{eq}(i,j)\cdot\sigma_0(j)\right)^2. \qquad (3.15)$$

The standard deviation of closure force along the mating edge is then the square root of the variance. The results of this calculation are shown in Figure 3.3, where the standard deviation of the closure force in the vertical direction is plotted for each fastener node.

The example assembly problem was analyzed again, with the parts meshed into a

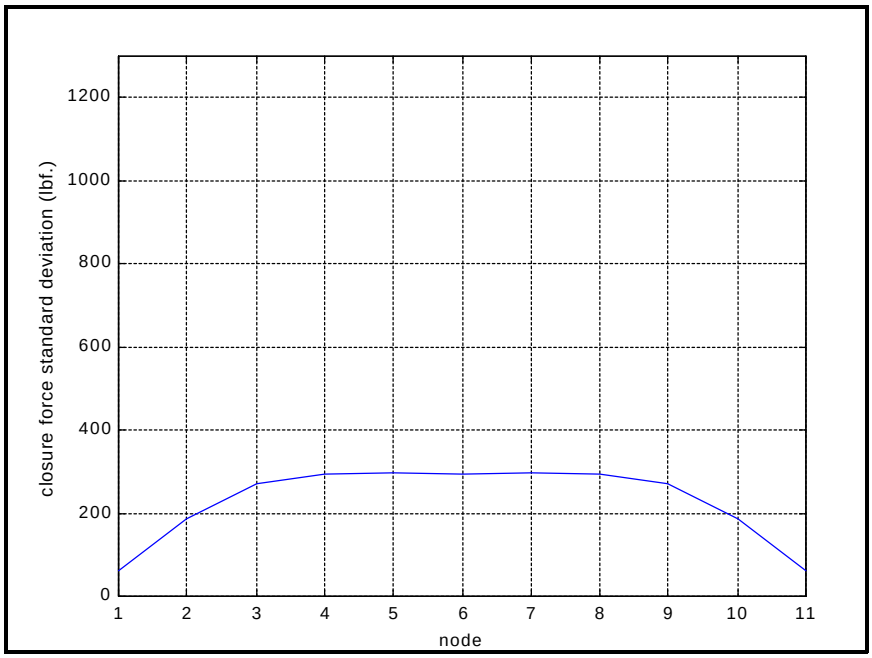

Figure 3.3 Standard deviation of closure force, 10 by 10 mesh

40 by 40 grid of elements. Every one of the 41 pairs of nodes along the mating edges represented a fastener. The stiffness matrices for the two parts were again condensed into super-elements and combined into one equivalent stiffness matrix. Because closure forces were only applied at fastener nodes, the resulting stiffness matrix equation was partitioned and solved for only the 41 vertical degrees of freedom at fastener nodes. The standard deviation of the closure force for this case is plotted in Figure 3.4.

The closure force, and therefore the standard deviation of closure force, at each fastener was expected to be less for the finer mesh because there were more fasteners closing the gap. As can be seen, however, the predicted standard deviation for the 40 by 40 element mesh is much higher than for the 10 by 10 mesh. This discrepancy arises from assuming that each nodal variation is independently random. In reality, the nodal variations are not independent, and the covariance between them must be included to

model the assembly statistically. Sources of this covariance will be discussed next.

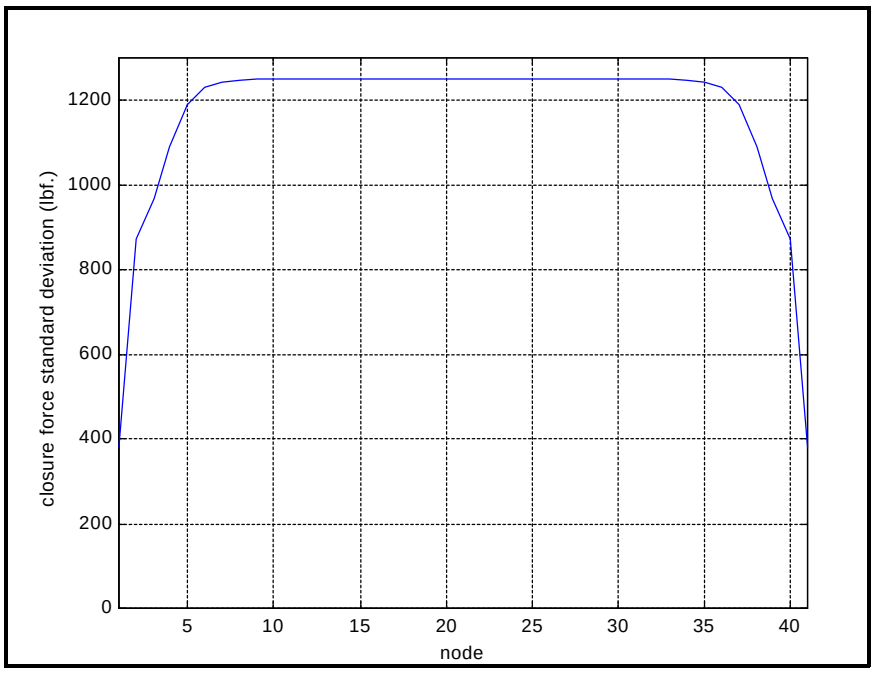

Figure 3.4 Standard deviation of closure force, 40 by 40 mesh

3.5 Material Covariance

Covariance between nodal displacements in the finite element model must be included in a statistical analysis, because the random displacements are not independent variables. Merkley (1996) showed that Monte Carlo simulations of finite element flexible assembly models are in error if nodal variations are assumed to be independently random variables. Material elasticity relates the displacements of neighboring nodes through the stiffness matrix. As shown in Figure 3.5, if a force displaces node *i*, surrounding nodes are also displaced due to material coupling. The displacement of all nodes due to a force on node *i* can be solved using the finite element stiffness equation:

$$\begin{Bmatrix} \delta_0 \\ \vdots \\ \delta_i \\ \vdots \\ \delta_n \end{Bmatrix} = \left[K^{-1}\right] \begin{Bmatrix} 0 \\ \vdots \\ F_i \\ \vdots \\ 0 \end{Bmatrix}.$$

Merkley called this coupling of nodal displacements through the stiffness matrix “material covariance” (Merkley 1998).

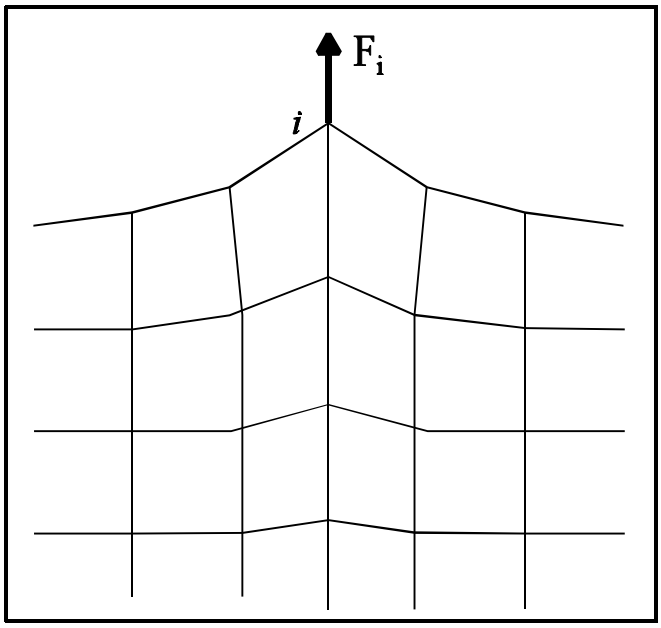

Figure 3.5 Material coupling of nodes.

3.6 Geometric Covariance

Merkley further explained that nodal variations on a surface are not independent, but are related through surface continuity constraints (Merkley 1998). If two nodes on a surface are deviated to one side of nominal, as in Figure 3.6, a node between them is likely to also be deviated to the same side. The variation of one node affects the probability distribution of surrounding nodes. This influence on surrounding nodes diminishes as

distance between the nodes increases. Merkley called the interrelation of nodal variations due to surface continuity “geometric covariance.”

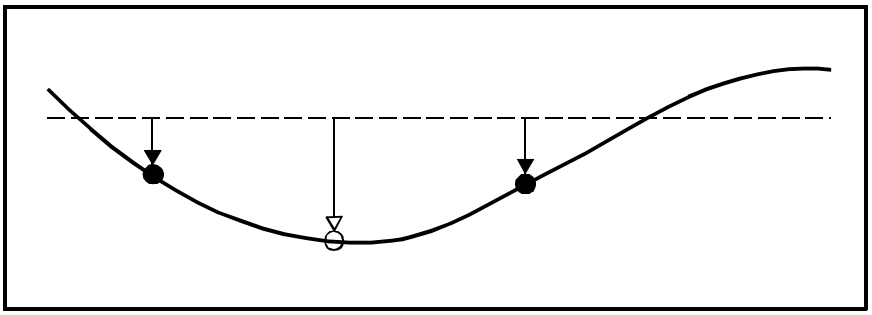

Figure 3.6 Geometric covariance.

3.7 Statistical Analysis of a Finite Element Model

The mean and standard deviation of assembly forces and stresses can be calculated from the equivalent stiffness matrix using statistical information about the gap between mating surfaces. The mean closure force vector μ_F can be evaluated from the definition of the mean, using the statistical expected value operator E[]:

$$\{\mu_F\} = E[\{F\}] = E\left[\left[K_{eq}\right]\{\delta_0\}\right].$$

And, because the stiffness matrix is not random,

$$\{\mu_F\} = \left[K_{eq}\right] E\left[\{\delta_0\}\right] = \left[K_{eq}\right]\{\mu_0\}, \tag{3.16}$$

where μ_0 is the mean gap vector. This shows that the mean closure force vector is linearly proportional to the mean gap vector.

The covariance matrix of the closure forces, $Ó_F$, can also be evaluated from the definition of the covariance matrix (see Section 4.4):

$$\left[\Sigma_F\right] = E\left[\left(\{F\} - \{\mu_F\}\right)\left(\{F\} - \{\mu_F\}\right)^T\right]$$

$$= E\left[\left(\left[K_{eq}\right]\{\delta_0\} - \left[K_{eq}\right]\{\mu_0\}\right)\left(\left[K_{eq}\right]\{\delta_0\} - \left[K_{eq}\right]\{\mu_0\}\right)^T\right],$$

$$= E\left[\left[K_{eq}\right]\left(\{\delta_0\} - \{\mu_0\}\right)\left(\left[K_{eq}\right]\left(\{\delta_0\} - \{\mu_0\}\right)\right)^T\right],$$

$$= E\left[\left[K_{eq}\right]\left(\{\delta_0\} - \{\mu_0\}\right)\left(\{\delta_0\} - \{\mu_0\}\right)^T\left[K_{eq}\right]^T\right],$$

And again, because the stiffness matrix is not random,

$$= \left[K_{eq}\right] E\left[\left(\{\delta_0\} - \{\mu_0\}\right)\left(\{\delta_0\} - \{\mu_0\}\right)^T\right]\left[K_{eq}\right]^T$$

$$\left[\Sigma_F\right] = \left[K_{eq}\right]\left[\Sigma_0\right]\left[K_{eq}\right]^T, \qquad (3.17)$$

where $Ó_0$ is the covariance matrix of the gap vectors, which describes the effects of geometric covariance. By multiplication with the stiffness matrix, the force covariance matrix $Ó_F$ includes both the effects of material and geometric covariance described above. The diagonal terms of a covariance matrix represent the variance of the variables involved. Therefore, if the nodal variations were independent, so there was no covariance, the gap vector covariance matrix would be a diagonal matrix. And, the standard deviation of the closure forces can be obtained by taking the square root of the diagonal terms in the force covariance matrix.

Using this derived relation between the covariance matrix of the gap vectors and the covariance of the closure forces, statistical assembly results can be predicted very efficiently. Although the mean and covariance of a population of gap vectors must be calculated for input into Equations 3.16 and 3.17, Monte Carlo simulation requires similar

calculation of the statistical descriptors of output results, such as the mean and standard deviation of closure force. Using the mean and covariance of a measured or simulated population of gap vectors as input requires evaluating only two matrix equations to obtain the mean and standard deviation of closure force. Because the finite element model of an assembly is a linear model, results from both methods are identical for a given population of gap vectors. The proposed FASTA method uses a gap covariance matrix as input for predicting assembly results. Compared to the enormous number of finite element calculations required to perform an equivalent Monte Carlo simulation, the FASTA method involves far less computation. As will be seen, however, the FASTA method does not necessarily require a population of gap vectors as input.

Chapter 4

COVARIANCE FROM SPECTRAL ANALYSIS

Because a geometric covariance matrix relating nodal displacements is needed for statistical finite element analysis, simple tolerance bands are not sufficient to describe surface variations. Surfaces must be further characterized such that their geometric covariance can be defined. Stout (unpublished) modeled surface profiles using polynomial curves, and showed that the wavelength of surface variations has a significant effect on geometric covariance and resulting statistical assembly results. The frequency content of surface variations must therefore be defined in order to find a relationship between variation wavelength and flexible assembly results. Spectral analysis of surface variations provides a direct method for obtaining the geometric covariance matrix.

4.1 Typical Surface Variations

Typical surface profiles contain variations from multiple sources, each producing variations having a certain range of wavelength. Figure 4.1 shows an example surface profile, scanned from an actual sheet metal part using a CMM (Coordinate Measuring Machine). Such surface variations typically have random phase, so the peaks of the surface can occur anywhere. Tolerance bands are therefore imposed on surfaces to limit

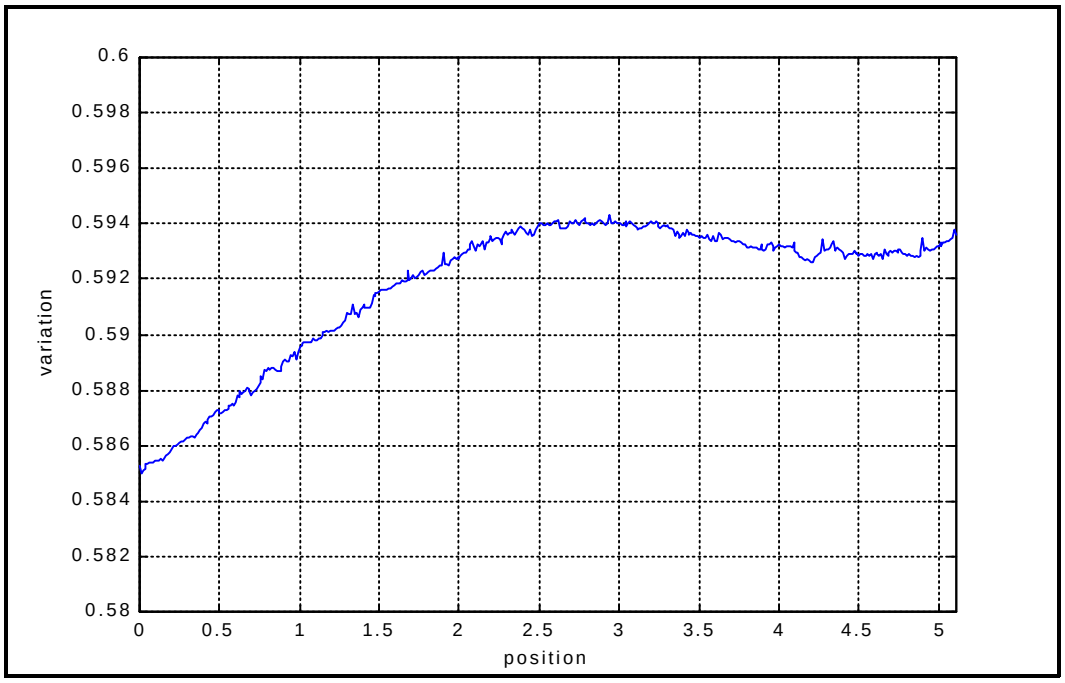

Figure 4.1 Example surface scan (Soman, unpublished).

the peak amplitude of surface variations. But, tolerance bands do not include any information about the wavelength of surface waviness. Because the wavelength of variation affects assembly results, tolerances on flexible parts should also describe the allowable frequency content of surface variations. Spectral analysis is commonly used to represent the frequency content of surfaces (Thomas 1982). Performing a Fourier transform on surface data, as discussed below, gives the frequency content of the surface. This is useful in identifying sources of variation and their relative magnitude, as well as calculating the geometric covariance of a surface for statistical analysis.

4.2 Surface Variation Model

The proposed FASTA method models surface variations as a finite summation of discrete sinusoidal waves, each with a different amplitude and wavelength. Any surface

profile can be modeled as a summation of sinusoids having different wavelengths and amplitudes, and represented in the frequency domain using the Fourier transform. Representing part surfaces in the frequency domain allows a simple derivation of the geometric covariance matrix from the autospectrum (or autospectral density) function used in spectral analysis. The autospectrum function has been used to communicate statistical information about random surface variations (Thomas 1982). As will be shown, spectral analysis techniques are also useful for representing surface variations in finite element flexible assembly models.

Surface variations may be modeled as *discrete, stationary* random processes which can be analyzed using modern spectral analysis methods. For finite element analysis of flexible assemblies, surface variations and displacements only need to be defined at nodal locations. Therefore, surface variations can be modeled as *discrete* (digital) processes, only having values corresponding to nodes in the finite element model. For discrete processes, the Fourier transform is a finite summation of sinusoids with discrete frequencies. Therefore, the frequency spectrum is discrete also. Discrete process data can be easily transformed and evaluated by computer, making it convenient to use with finite element models.

A *stationary* process is one for which the probability distribution function is the same at any point along the process. All statistical moments obtained from a population of processes, such as the mean and standard deviation, are assumed to be constant along the entire process. While part surfaces of finite length do not fit the theoretical definition for stationary processes, they can be modeled as samples taken from an infinitely long surface.

As explained below, the mean and variance of surface variations must be assumed stationary to form a covariance matrix from the autocorrelation function. This assumption is valid for a surface if all variations have a uniformly-random phase distribution, and if the frequency content of the variations does not change along the surface.

4.3 Autocorrelation Function

For random processes which are functions of distance, such as random variations along part surfaces, the autocorrelation function describes the relation between process values at different locations. When applied to surface variations at boundary nodes in a finite element model, it describes the covariance between nodes due to all wavelengths of variation in the part surface.

The *autocorrelation* function is the expected value, averaged over a population of processes, of the product of two points separated by a given distance. The autocorrelation function $R_u(\zeta)$ of a population of processes u(x), where u is a function of distance x, is defined using *E*[], the statistical expected value operator, as

$$R_u(\zeta) = E\left[u(x)u(x+\zeta)\right] = \frac{1}{n}\sum_{i=1}^{n}\sum_{j=1}^{n} u_i(x)u_j(x+\zeta). \qquad (4.1)$$

In this definition, x and x+æare two points in the process separated by the distance æ

For discrete processes, the autocorrelation function can be evaluated much more efficiently by using the Fast Fourier Transform (FFT) algorithm commonly found in mathematics and signal-processing software, rather than from the above definition. The FFT algorithm quickly transforms discrete data into the frequency domain. First, known

data points are transformed into the spatial frequency domain using the FFT. They are represented as complex numbers having phase and amplitude at discrete frequencies. The transformed data is then multiplied by its conjugate to form the auto-spectral density function (also known as the *autospectrum* or power spectral density). The data is then inverse transformed back into the space domain to obtain the *autocorrelation* function. A derivation of this method can be found in most spectral analysis texts, and is beyond the scope of this paper (Thornhill 1994). Figure 4.2 shows an example process, the amplitude of its Fourier transform, its autospectrum, and its autocorrelation function.

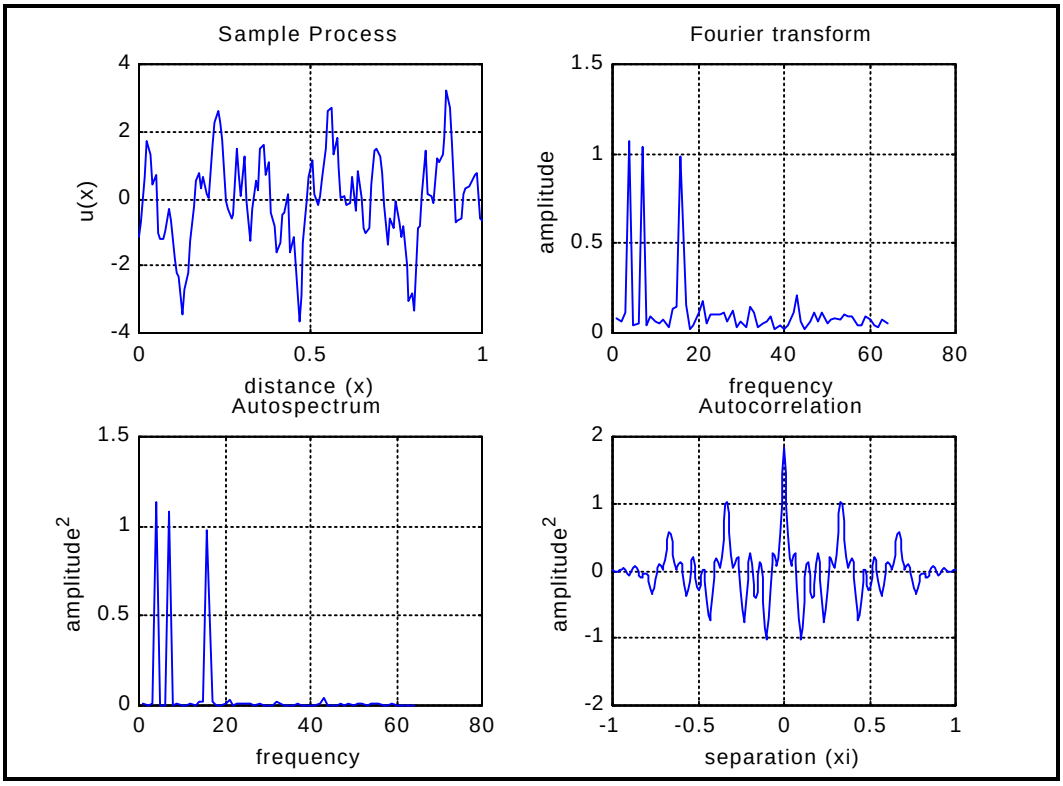

Figure 4.2 Fourier transform, autospectrum, and autocorrelation of sample process.

Because the FFT algorithm transforms processes into discrete frequencies, using it to evaluate the autocorrelation function assumes that all wavelengths in a process are

evenly divisible into the sample length. In other words, it assumes that the process is periodic within the sample length, and repeats itself outside this range. One result of this assumption is called “circular correlation”, because the assumed periodicity can be visualized as wrapping the data into a circle, with the end joined to the beginning. If circular correlation is not desired, zeros can be added to the end of the data to cancel any terms resulting from circular correlation. This causes the amplitude of the resulting autocorrelation sequence to decay linearly toward the end of the data. Another method for obtaining the autocorrelation sequence is to pad with zeros as above, then scale the results such that the amplitudes do not decay. Each of these methods gives a different result. The method used depends on what assumptions are made about the process, i.e. whether or not the process is assumed to be periodic.

4.4 Geometric Covariance Matrix

The covariance, C, of two random variables x and y is defined as the expected value of their product after the mean values of the two variables, μ_x and μ_y, have been subtracted:

$$C(x,y) = E\left[\left(x-\mu_x\right)\left(y-\mu_y\right)\right] = \frac{1}{n}\sum_x\sum_y\left(x-\mu_x\right)\left(y-\mu_y\right). \quad (4.2)$$

The autocorrelation function for two points in a population of processes can be related to their covariance. This requires assumptions about the stationarity of the processes as mentioned earlier. The mean of the population of processes must be stationary along the

process. Also, the covariance of the population must be assumed to be the same at any point along the processes.

The covariance, $C_u(x,\zeta)$, between any two points, x and $x+\zeta$, in a process u(x) is:

$$C_u(x,\zeta) = E\left[\left(u(x) - \mu(x)\right)\left(u(x+\zeta) - \mu(x+\zeta)\right)\right], \tag{4.3}$$

where $\mu(x)$ is the process mean at the two points. The covariance is a function of both location, x, and separation, ζ. If the covariance is assumed to be stationary, it is the same at any location along the process, and is only a function of separation distance:

$$C_u(x,\zeta) = C_u(\zeta)$$

If the mean of the process is also assumed to be stationary, it is the same at any point along the process, so

$$\mu(x) = \mu(x+\zeta) = \mu .$$

The expression for covariance, Equation 4.3, can be evaluated using these assumptions:

$$\begin{aligned} C_u(\zeta) &= E\left[\left(u(x) - \mu\right)\left(u(x+\zeta) - \mu\right)\right] \\ &= E\left[u(x)u(x+\zeta)\right] - \mu E\left[u(x)\right] - \mu E\left[u(x+\zeta)\right] + \mu^2 . \end{aligned}$$

Because the mean of the process, μ, is defined as the expected value of the process u(x),

$$\begin{aligned} &= E\left[u(x)u(x+\zeta)\right] - 2\mu^2 + \mu^2 \\ &= R_u(\zeta) - \mu^2 \end{aligned}$$

from Equation 4.1. The autocorrelation, $R_u(\zeta)$, of two points in a process is then related to the covariance of the process, $C_u(\zeta)$, by

$$R_u(\zeta) = C_u(\zeta) + \mu^2 , \tag{4.4}$$

where μ is the mean of the process (Bendat 1986). If the process mean is zero, the autocorrelation and covariance functions are equal.

4.5 Direct Calculation of the Geometric Covariance Matrix

The covariance function defined in Equation 4.2 can be used to form a matrix of covariances directly from a population of processes. This matrix is called the covariance matrix, and it completely describes the covariance of all points in a random process. When used to describe surface variations for a population of surfaces, the matrix formed is the *geometric covariance matrix* from Chapter 3. Each term in the matrix represents the expected value of the product of the variations at two different points along the surface. The covariance between every possible pair of points is included in the matrix. Diagonal terms in the covariance matrix represent the expected squared value of variation at each point (the product of the variation and itself), or the variance at each point. Other terms off the diagonal represent the covariance between variation at points spaced increasingly apart. The geometric covariance matrix is used to predict statistical assembly results from a finite element model.

Surface variation data from a population of surfaces can be used to calculate the geometric covariance matrix directly, through simple matrix operations. Surface profile data for each of *n* parts in a population are placed into column vectors. The mean surface vector of the population is calculated and subtracted from each surface profile vector in the population. The resulting column vectors contain only random variations, which are the difference between each surface and the mean surface. The column vectors of random

variations can be arranged into a matrix, $\hat{X}$, and the covariance matrix of the population of *n* surfaces can be easily calculated from the matrix multiplication:

$$\left[\Sigma_X\right] = \frac{1}{n}\left[\hat{X}\right]\left[\hat{X}\right]^T . \tag{4.5}$$

This series of matrix operations forms a covariance matrix with each term calculated according to the definition of covariance in Equation 4.2 (Johnson 1988). This method of obtaining the geometric covariance matrix will be referred to as the "direct statistical method". Statistical assembly results using this covariance matrix as input are identical to results obtained from a Monte Carlo simulation, because the finite element matrix equations are linear operations. Calculating the covariance of the input gap vectors and using covariant finite element relations, such as Equation 3.17, is equivalent to calculating the covariance of the output forces, deformations, or stresses after solving the finite element equations for each input individually.

The covariance or autocorrelation of a population of gaps between two mating surfaces in an assembly can be found from the covariance or autocorrelation of each individual population of surfaces. Because the variations in one population of surfaces can be assumed independent from variations in the other population, the covariance of the gaps is simply the sum of the covariance of each surface population. For two populations of surfaces A and B, the population of gaps is the difference between each population of surfaces. The covariance of the gap is then

$$C(A - B) = C(A) + C(B) . \tag{4.6}$$

4.6 Calculation of the Geometric Covariance Matrix from Autocorrelation

The geometric covariance matrix can also be constructed from the average autocorrelation function of a population of surfaces. The diagonal variance terms in the covariance matrix correspond to the autocorrelation sequence at zero separation (æ=0). The off-diagonal terms represent the covariance between two nodes spaced some distance apart. This is similar to the autocorrelation function evaluated for two nodes at a given separation. To transform the autocorrelation sequence into the covariance matrix, the sequence must be shifted to form each row of the matrix, so the correlation at zero separation (a node with itself) lies on the diagonal. Figure 4.3 depicts this shifting. The other points in the autocorrelation sequence then represent the covariance between nodes spaced increasingly apart. The nodes are normally assumed to be evenly spaced. If they are not, the autocorrelation sequence must be interpolated to the proper nodal spacing, and the value entered into the corresponding covariance term in the covariance matrix.

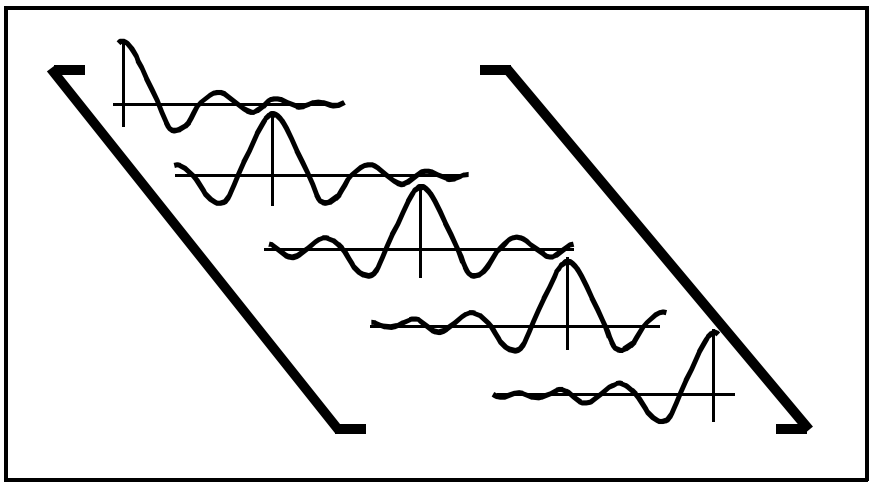

Figure 4.3 Shifting the autocorrelation sequence to form rows of the geometric covariance matrix.

Forming the covariance matrix in this way assumes again that the covariance of surface variations is stationary. Because each row of the covariance matrix is formed from the same autocorrelation sequence, the covariance between two points separated by a given distance is assumed to be independent of position along each surface. The variance, and therefore the standard deviation, of surface variation is also assumed to be the same at each node. This implies a constant-width standard deviation band, offset from the mean surface, similar to those used to place tolerances on surfaces of rigid parts.

4.7 Deterministic versus Random Variation

Surface variations are often assumed to be completely random. For purely random variations, if a large population of random surfaces is averaged, the mean surface will be zero. However, some processes produce parts which have non-random, or deterministic, variations. If a large population of these parts is averaged, there will be a mean variation common among all of them. Such variation may result from warping of composite parts, errors in dies or tooling used to produce the parts, or any repeatable error in the manufacturing process which produces parts biased from the nominal geometry. From a frequency point of view, random variations would have uniformly random phase, while the deterministic variations would have similar phase from part to part. When performing a tolerance analysis of flexible assemblies, it is important to account for both types of variation.

Given a population of surfaces, the proposed FASTA method averages all the surface data over the population to find a vector representing the mean surface. The mean

surface will deviate from nominal if each part has similar variation. The resulting mean surface is then subtracted from each surface in the population to leave only random variations. This procedure allows separation of deterministic variations, which have similar phase, from random variations, which have random phase. This is important, because the autospectrum and autocorrelation functions do not contain information about the phase of variations in the surface, and assume uniformly-random distributed phase. Subtracting the mean surface also satisfies the assumption that the mean of the surfaces is stationary, making the mean of the resulting population zero everywhere along the surface. Any variation from the mean surface is included in the autocorrelation of the random variations. Separation of mean and random variation requires two FEA solutions. The mean surface is used in the finite element model to calculate the mean assembly results, and the autocorrelation of the random variations is used in the calculation of the range of variation of the assembly results.

4.8 Average Autospectrum

To avoid performing the inverse Fourier transform for each surface when computing the average autocorrelation sequence of a population, the autospectrum of each surface is calculated, and the average autospectrum is inverse transformed to give the average autocorrelation. Because the Fourier transform is linear, the results are the same. This method requires only one inverse Fourier transform. This modification greatly reduces the run-time of the FASTA method.

4.9 Procedure

In summary, the procedure followed to predict the mean and standard deviation of assembly results for two populations of parts is:

1. Construct a finite element model of the parts, based on nominal geometry.
2. Condense the stiffness matrices to involve only boundary-node terms.
3. Combine the stiffness matrices of the parts into one equivalent stiffness matrix for the assembly.
4. For each population of surfaces, calculate the mean surface.
5. Subtract the two mating mean surfaces to calculate the mean gap, and use it in the finite element model to predict mean assembly results.
6. Subtract the mean surface from each surface in the populations, and compute the average autocorrelation sequence of each population.
7. Add the two average autocorrelation sequences to form the autocorrelation of the gap.
8. Construct the geometric covariance matrix from the average autocorrelation sequence of the gap.
9. Use the geometric covariance matrix in the finite element model to predict the standard deviation of assembly results.

The average autocorrelation sequence of the gap may be calculated by first subtracting the two populations of surfaces to form a population of gaps. But, the autocorrelation of each population contains useful information about the variations in that

particular population. For controlling assembly results, it is better to calculate the autocorrelation for each population separately.

Chapter 5

VERIFICATION OF THE FREQUENCY ANALYSIS METHOD

To verify the FASTA method, the simple lap joint problem presented in Chapter 3 was analyzed by both Monte Carlo simulation and by the frequency analysis method and the results compared. In this problem, only two mating part edges must be joined (see Figure 3.2). A population of 5,000 gaps between the mating edges was simulated by superimposing random sine curves of several different wavelengths. This is equivalent to generating two populations of random surfaces and subtracting them to find the gap. The wavelength, relative amplitude, and phase of the sinusoids used to create this population are listed in Table 5.1 below. Both random and non-random variations were included in

Table 5.1 Sinusoids used to create simulated population of gaps.

Wavelength/edge length ratio	Relative amplitude distribution	Phase distribution
1/2	Normal, mean = 1, std. dev. = 1	Normal, mean = 0, std. dev. = 0.2ð
1/4	Normal, mean = 1/2, std. dev. = 1/2	Uniform, 0 to 2ð
1/10	Normal, mean = 1/4, std. dev. = 1/4	Uniform, 0 to 2ð

the simulated gaps. The random variations have uniformly-distributed phase, while the variation with normally-distributed phase simulates a non-random, mean variation. Each gap was scaled to have a standard deviation of 0.033 inches. The same simulated gap data was used as input for both methods.

Each method was used to predict the expected range of closure forces required to close the gap along the mating edges. Every node along the mating edges represented a fastener. The frequency analysis method used the mean gap and average autocorrelation of the gaps as input into the finite element model, while the Monte Carlo simulation performed a finite element analysis for all 5,000 random gaps. The two parts were modeled in their nominal shape and meshed into a 40 by 40 grid of bending-only plate finite elements. Again, the individual stiffness matrices were condensed to involve only boundary degrees of freedom, and combined into one equivalent stiffness matrix for the assembly. Vertical displacement boundary conditions along the mating edges were defined by the gap vectors, and the fixed edges were constrained in all three degrees of freedom.

5.1 Circular Correlation Method

The FASTA method was used to predict assembly forces when the gap was closed at each node. The statistical distribution of the gaps was evaluated using the autocorrelation sequence to determine the mean and standard deviation of the closure forces. Circular correlation was initially used for this analysis, because it is the simplest to compute.

Two finite element solutions were required, corresponding to the mean force and the force covariance. The mean closure force vector was calculated from the mean gap vector, as in Equation 3.16. The predicted mean closure force vector is plotted in Figure 5.1. The mean forces are caused by the non-random variations included in the simulated population of gap vectors. Because the non-random variations were periodic, periodicity also exists in the mean closure force.

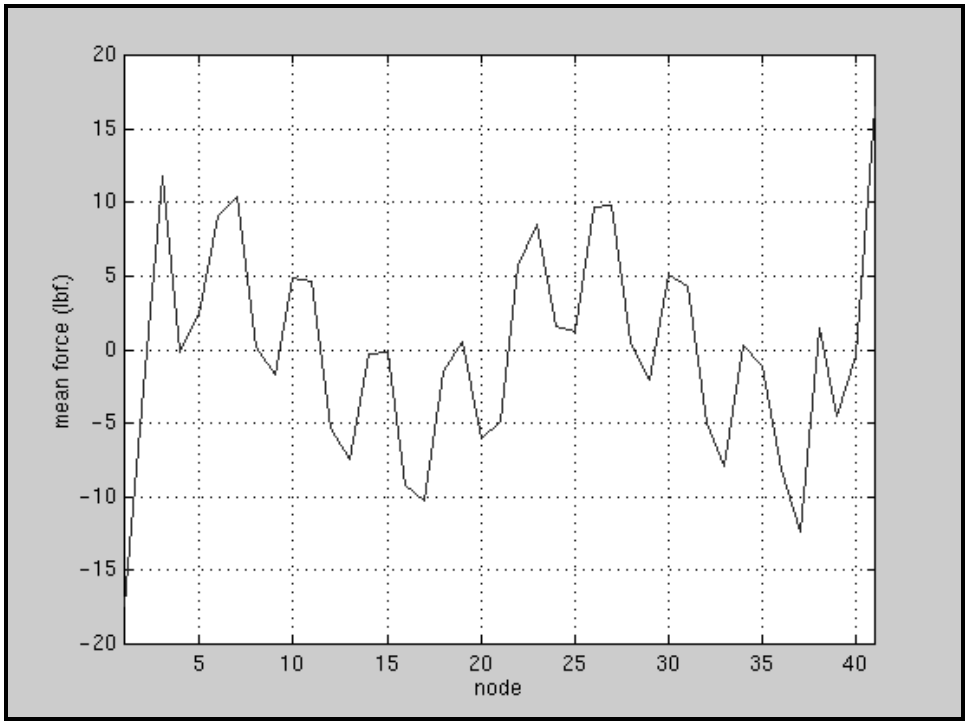

Figure 5.1 Mean closure force from circular correlation.

The geometric covariance matrix of the gaps was formed from the average circular autocorrelation function and used as input into the finite element model. The middle row of the covariance matrix, which is the center range of the autocorrelation of the gaps, is plotted in Figure 5.2. The center peak is the variance term, or a node correlated with itself. The periodicity of the autocorrelation is caused by the periodic

random variations in the population of gaps. Because the covariance is assumed stationary in this method, every row of the matrix is the same only shifted; therefore, the main diagonal and sub-diagonals each have constant amplitude.

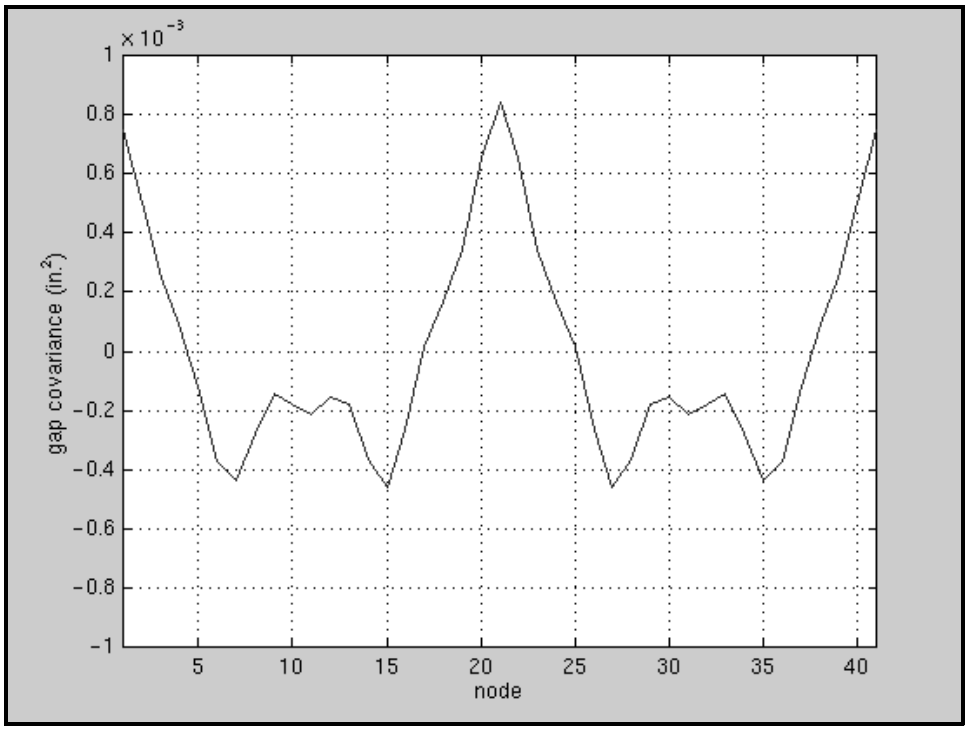

Figure 5.2 Middle row of gap covariance matrix from circular correlation.

The closure force covariance matrix was calculated from the gap covariance matrix by the covariant stiffness equation, Equation 3.17. The predicted force covariance matrix from this method is shown as a three-dimensional bar chart in Figure 5.3. The height of the bars represents the magnitude of each element in the matrix. The diagonal terms, running from left to right in the figure, represent the predicted variance of the closure forces. They have fairly uniform magnitude, which drops off at the corners of the matrix. To show the relative amplitudes of force variance and covariance terms, the middle row of the force covariance matrix is plotted in Figure 5.4 as a bar chart.

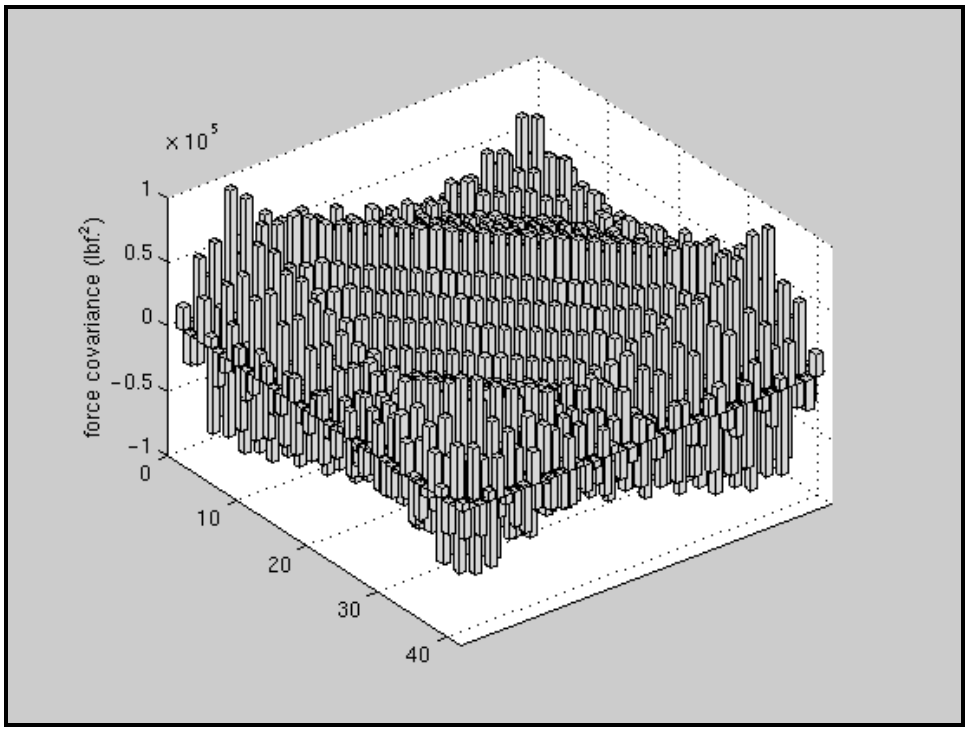

Figure 5.3 Closure force covariance matrix from circular correlation.

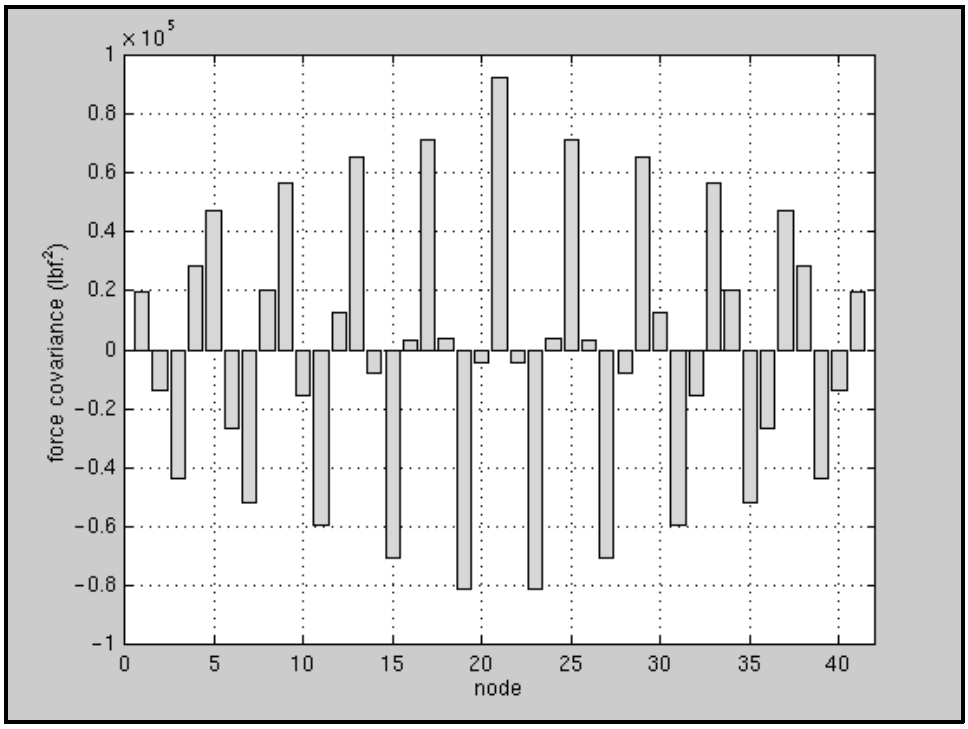

Figure 5.4 Middle row of closure force covariance matrix from circular correlation.

The magnitude of the force covariance terms are not periodic with the same frequency as the covariance terms in the input gap covariance matrix of Figure 5.2. The force covariance terms are periodic, but with a higher frequency than the gap covariance. These effects can be explained by examining the condensed equivalent stiffness matrix, shown as a bar chart in Figure 5.5. Because there are non-zero off-diagonal terms in the stiffness matrix, the periodic covariance of the gap is "smoothed" by pre- and post-multiplying the gap covariance matrix with the stiffness matrix. The terms in the stiffness matrix alternate from positive to negative, causing the high-frequency periodicity in the force covariance matrix. The periodicity in the stiffness matrix can be explained by observing that to displace only one node and leave all other nodes undisturbed, alternating positive and negative forces must be applied to surrounding nodes.

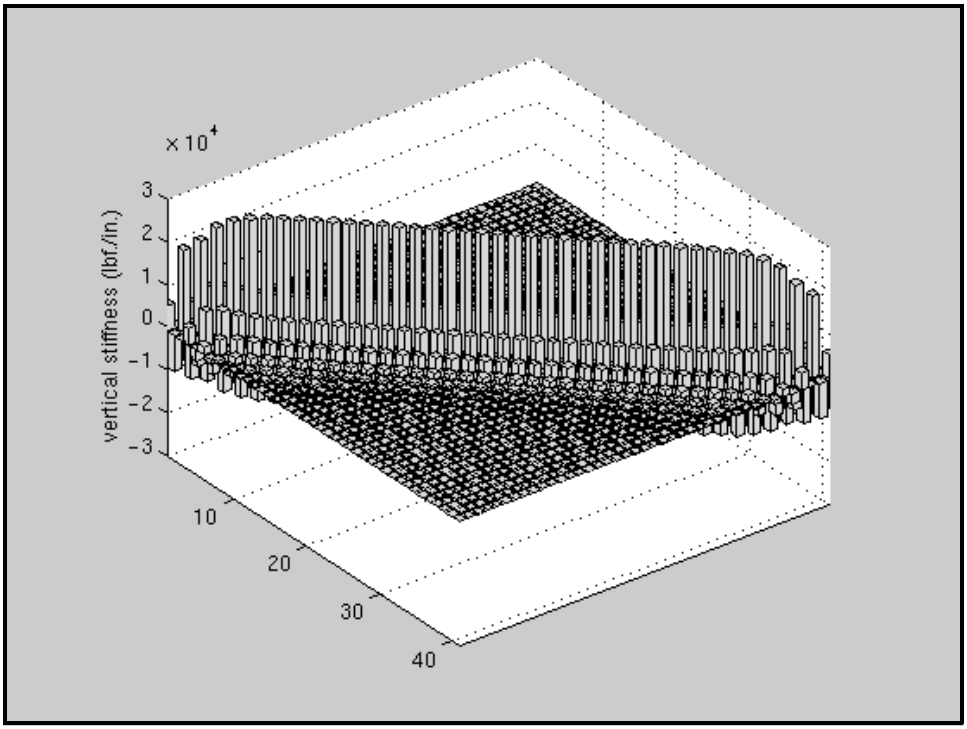

Figure 5.5 Condensed, equivalent stiffness matrix for lap-joint assembly.

The principal interest in this problem is the standard deviation of the closure forces, which is the square root of the diagonal, or variance, terms in the force covariance matrix. The standard deviation of the closure force vector predicted from the circular correlation method is plotted in Figure 5.6. For this particular case, the standard deviation of the closure force vector is greater than the mean force vector. But this is due to the nature of the input population of gap vectors, which have random variations larger than the mean variation.

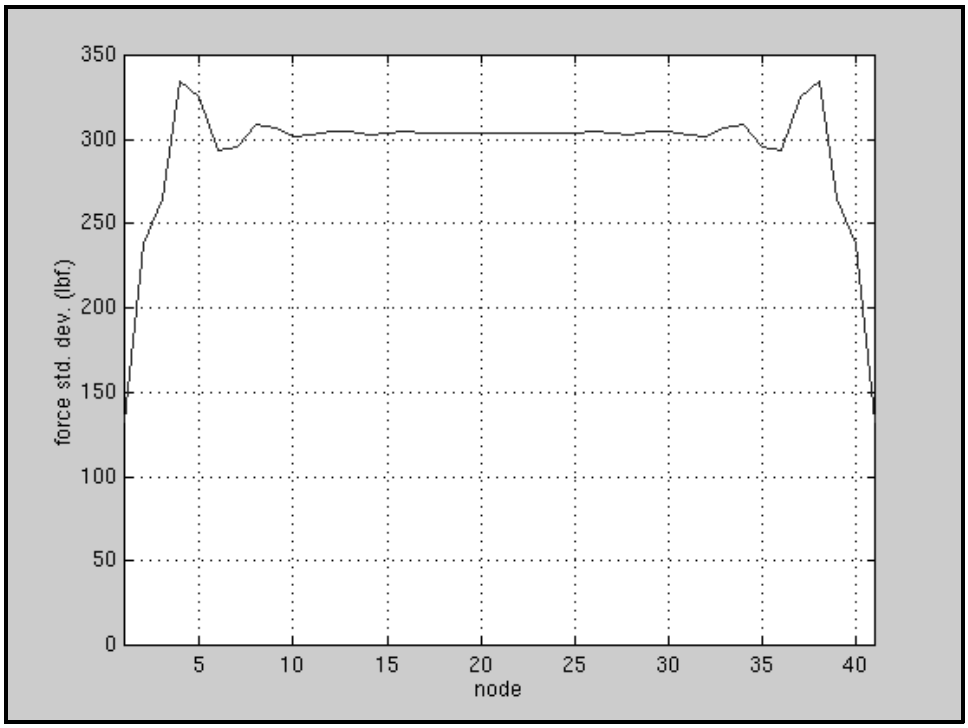

Figure 5.6 Standard deviation of closure force from circular correlation.

5.2 Monte Carlo Simulation

A Monte Carlo simulation was also performed using the same population of gaps. One finite element solution was required for each of the 5,000 gaps, using the same condensed, equivalent stiffness matrix for each case. The mean closure force and force

covariance matrix were calculated from the resulting 5,000 instances of closure force. Typical Monte Carlo simulations generate random numbers as input into a model, and store the results for statistical interpretation. Because of the covariance between points on a part surface, however, Monte Carlo simulations of flexible assemblies must generate random *surfaces* as input into a finite element model to include geometric covariance effects.

The mean closure force predicted by the Monte Carlo method was the same as that predicted by circular correlation. All methods used, including those described below, predicted the same mean closure force vector. This is because the finite element analysis is a linear operation, and using the mean gap vector as input is equivalent to calculating the mean of the force results.

The force covariance matrix from the Monte Carlo simulation is shown as a three-dimensional bar chart in Figure 5.7. Again, the height of the bars represents the magnitude of the terms in the matrix. Unlike the force covariance matrix predicted by the circular correlation method in Figure 5.3, the amplitude of the covariance terms in this matrix do not decay away from the diagonal. This can be seen in Figure 5.8, where the middle row of the force covariance matrix predicted by the Monte Carlo simulation is represented as a bar chart.

The predicted standard deviation of closure force, the square root of the diagonal variance terms, is plotted as a dashed line in Figure 5.9. To compare the results of the Monte Carlo simulation with those from circular correlation, the closure force standard deviation predicted from circular correlation is plotted again as a solid line in the same

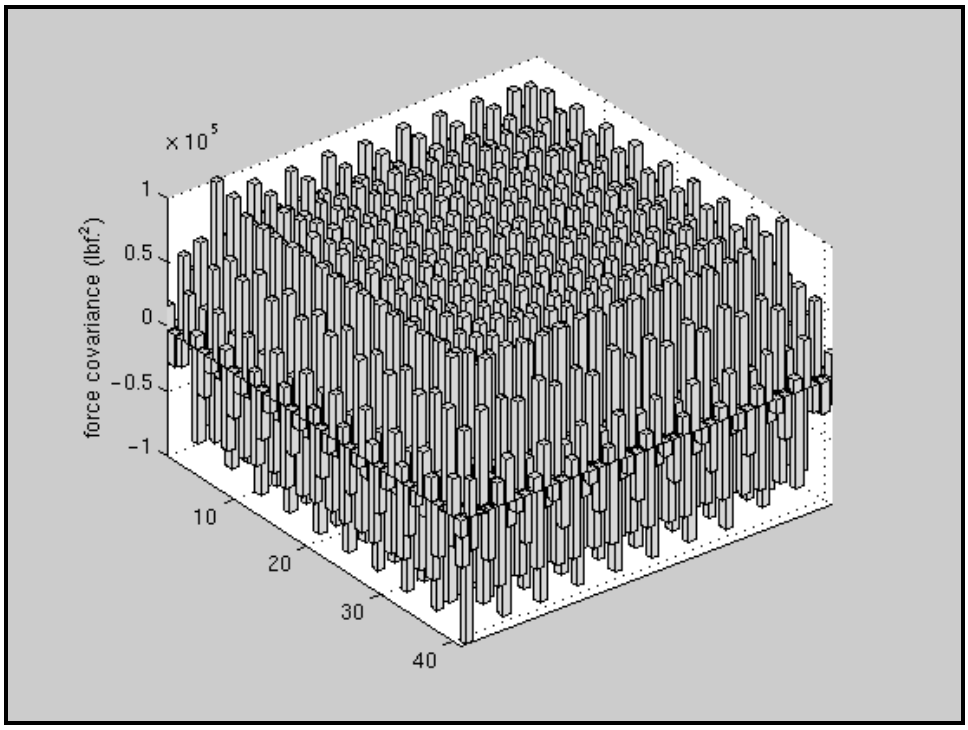

Figure 5.7 Closure force covariance matrix from Monte Carlo.

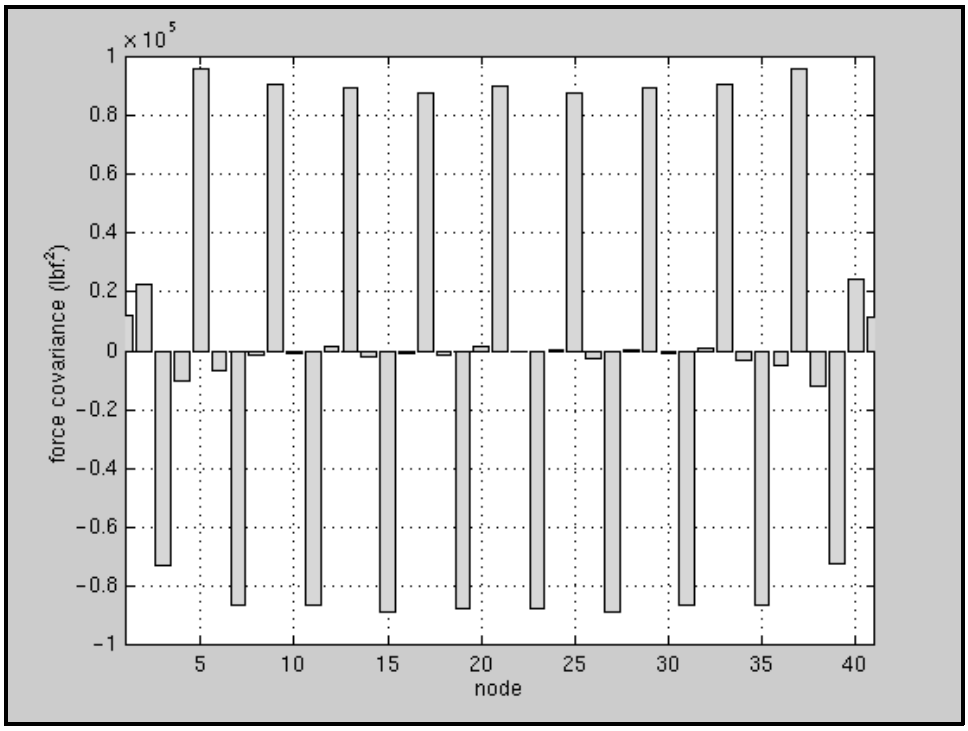

Figure 5.8 Middle row of closure force covariance matrix from Monte Carlo.

figure. The scale of this plot was increased to better show the difference between the two results. Although the force covariance terms are not similar, the force variance and standard deviation predicted by both methods agree very well.

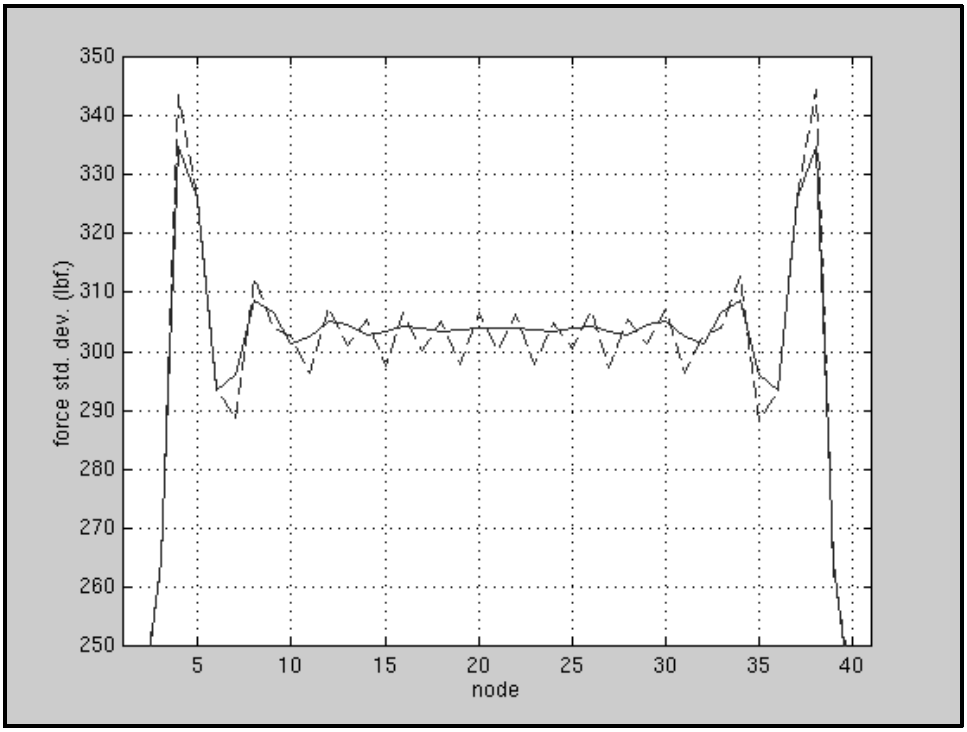

Figure 5.9 Closure force standard deviation from Monte Carlo (dashed) and circular correlation (solid).

Some difference can be seen between the force standard deviation predicted by the circular correlation and Monte Carlo methods. The standard deviation predicted by Monte Carlo simulation does not have as uniform magnitude as the circular correlation results. This is because the frequency analysis method uses an average autocorrelation sequence to form each row of the gap covariance matrix. The variance of the gap is assumed constant, and therefore the standard deviation of the closure force is more smooth than predicted by Monte Carlo.

5.3 Zero-Padded, Unbiased Autocorrelation Method

The covariance matrix of the input gap vectors was calculated again using the zero-padded, unbiased autocorrelation as explained in Section 4.3. The middle row of this gap covariance matrix, which is the center of the autocorrelation sequence, is plotted as a solid line with circles in Figure 5.10. To show the difference between the circular correlation gap covariance matrix and the zero-padded, unbiased correlation, the middle row of the gap covariance matrix from circular correlation is plotted again in Figure 5.10 as a plain solid line. The amplitudes of some covariance terms are slightly different between the two methods.

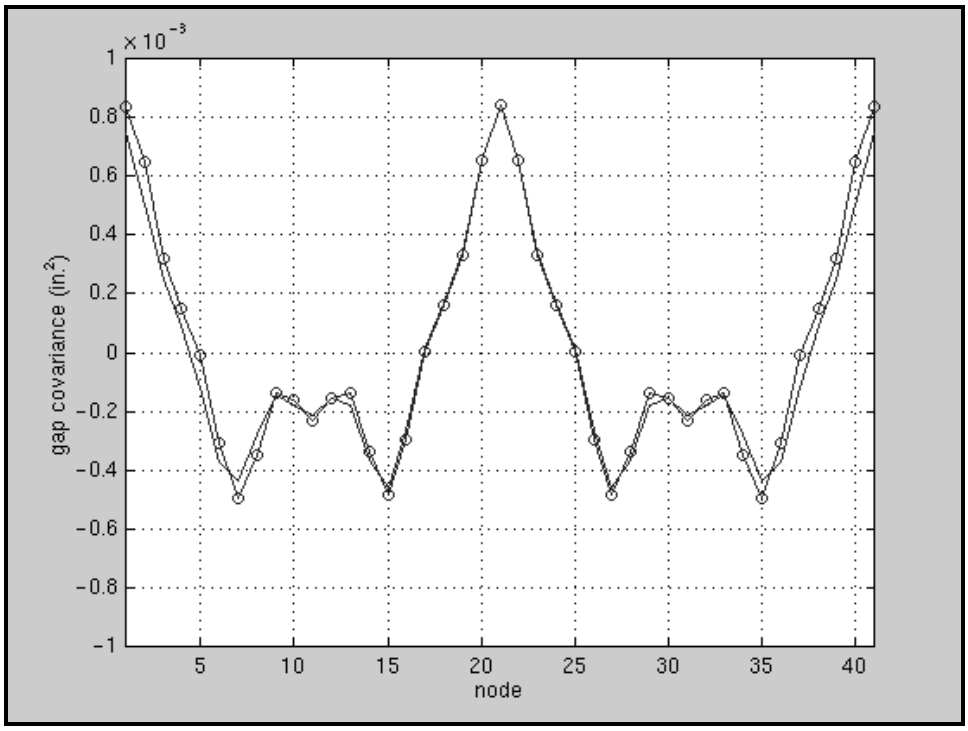

Figure 5.10 Middle row of gap covariance matrices from zero-padded, unbiased autocorrelation (solid, circles) and circular correlation (solid).

The gap covariance matrix from the zero-padded, unbiased method was used to again calculate the closure force covariance matrix. The closure force covariance matrix predicted by this method is shown in Figure 5.11 as a three-dimensional bar chart. The force covariance matrix from this method agrees better with the Monte Carlo results (Figure 5.7) than do the results from circular correlation.

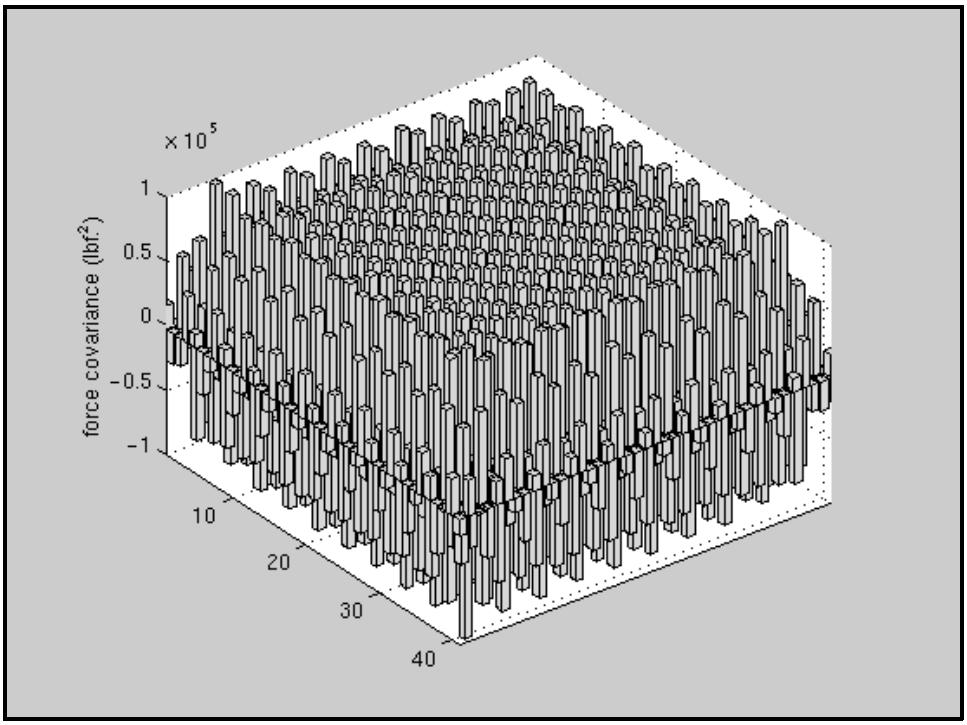

Figure 5.11 Closure force covariance matrix from zero-padded, unbiased autocorrelation.

The standard deviation of closure force predicted by zero-padded, unbiased autocorrelation is plotted as a solid line with circles in Figure 5.12, with the standard deviation from the Monte Carlo simulation shown as a dashed line. Again, the standard deviation scale has been reduced to better show the differences. As can be seen, although the two methods of calculating the autocorrelation function predicted different force

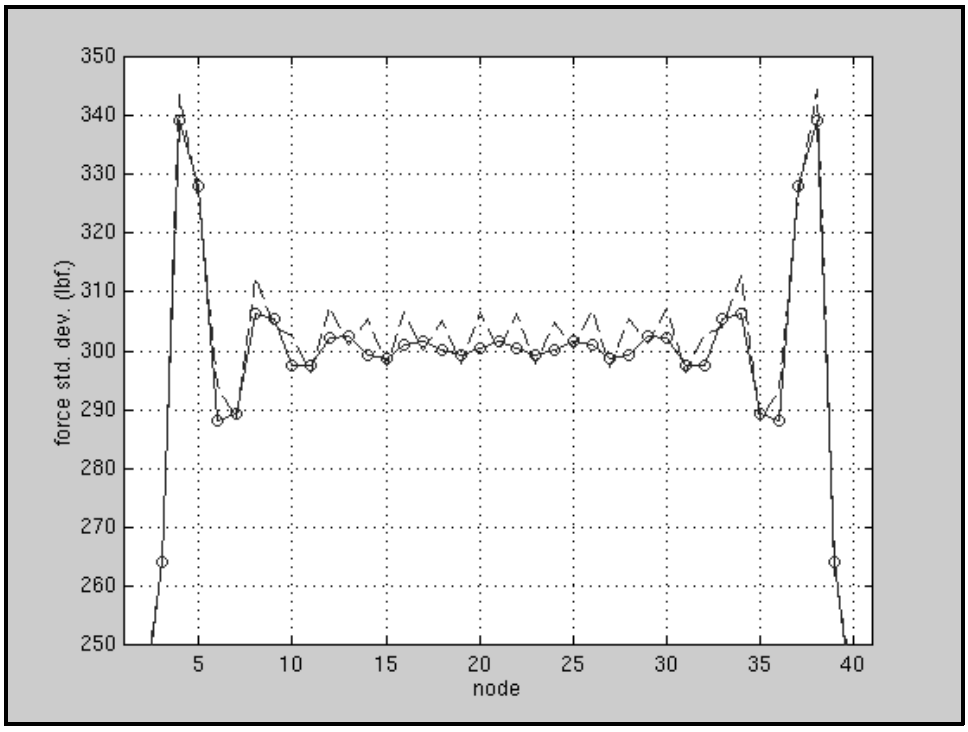

Figure 5.12 Closure force standard deviation from zero-padded, unbiased autocorrelation (solid, circles) and Monte Carlo (dashed).

covariance terms, both methods predicted force standard deviations which agree closely with Monte Carlo results. Because the stiffness matrix is banded (terms away from the main diagonal are very small), only the terms in the gap covariance matrix which are near the diagonal contribute significantly to the closure force variance. Since the circular correlation and zero-padded correlation sequences match well near the zero-separation term, the variances of the closure force calculated from each correlation are similar.

Both circular correlation and zero-padded correlation can give similar results if the autocorrelation is relatively small for separations greater than one half of the mating edge length. This could occur if the random variations in the part surfaces are non-periodic, or if the surfaces have many short-wavelength variations with relatively large amplitudes. Points along the mating edge which are separated by more than half the edge length would

not be significantly correlated. In this case, the circular correlation will be very similar to the zero-padded, unbiased correlation for separations between zero and one half the edge length. Zeros may be appended to the circular correlation sequence for separations over one half the edge length. This produces a correlation which is very similar to the correlation which would result from padding the surface variation data with zeros before performing the FFT.

Because circular correlation requires transforming a shorter sequence than does zero-padding, some computation time is saved by using circular correlation. But, the time required to perform an FFT is not great. To avoid errors due to circular correlation, therefore, it is recommended that *all* surface data be padded with zeros before transformation, and the average autocorrelation sequence be subsequently unbiased. Of course, the autocorrelation sequences may be examined for particular populations of parts to decide whether circular correlation can be used. The nature of the autocorrelation will depend on the manufacturing process used. Insufficient data exists on the autocorrelation of flexible part surfaces to predict in general which method should be used.

To demonstrate the higher accuracy of the FASTA method, a Monte Carlo simulation of 10,000 gaps was also performed. This larger number of samples is needed to obtain more accurate information from the Monte Carlo method. The standard deviation of closure force predicted by this Monte Carlo simulation is shown as a dashed line in Figure 5.13. The results showed even better agreement with the results from the unbiased autocorrelation method for 5,000 gaps, re-plotted as a solid line with circles. But, the simulation took 12.5 minutes, much longer than the FASTA method for similar

accuracy. The frequency analysis approach appears to be more accurate, more efficient, and does not require a large sample size for accuracy.

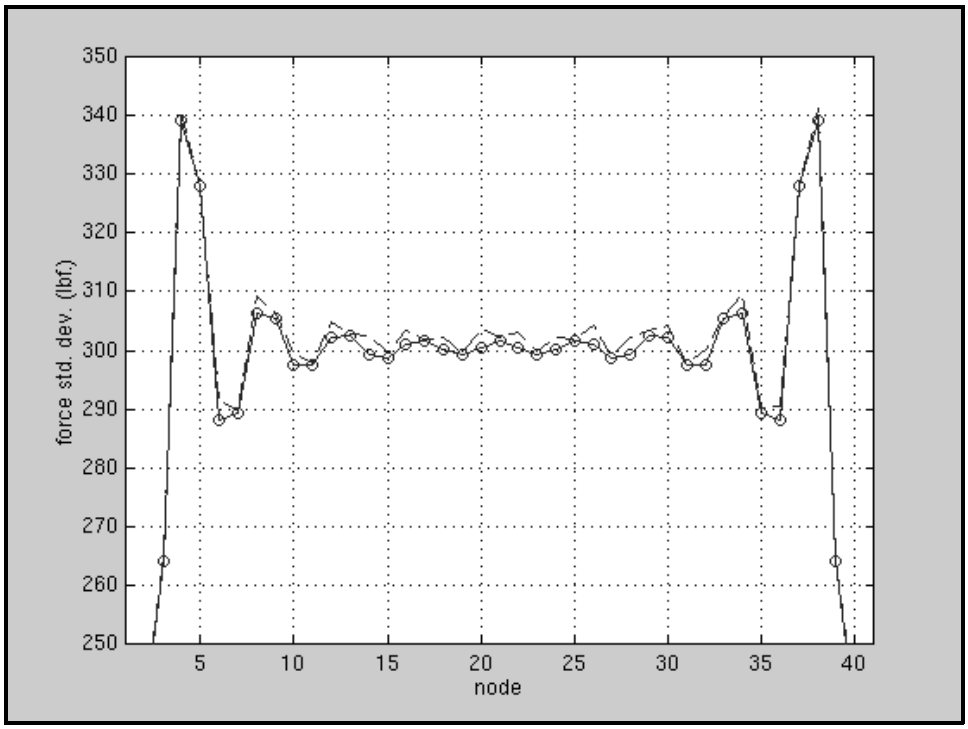

Figure 5.13 Closure force standard deviation from Monte Carlo with 10,000 samples (dashed) and zero-padded, unbiased autocorrelation with 5,000 samples (solid, circles).

5.4 Direct Statistical Method

In contrast to the Monte Carlo method, in which the force covariance matrix is calculated after the force has been calculated for each gap, the direct statistical method calculates the covariance matrix of the input gap vectors and uses it to calculate the force covariance matrix. The statistical method for calculating covariance matrices, described in Section 4.4, is used to calculate both the covariance of closure force results from the Monte Carlo method and the covariance of gap vector inputs in the direct statistical method.

If the direct method of calculating the geometric covariance matrix of a population of gap vectors is used as input into the finite element model, the results are identical to those from performing a Monte Carlo simulation on the same population. This is because the finite element model is linear, and all of the matrix equations used to evaluate the model are linear operations, as explained in Section 3.7. Comparing results from using direct statistical input and performing a Monte Carlo simulation is unnecessary, because they are equivalent. However, a Monte Carlo simulation involves solving the finite element equations once for *every* gap in the population and then calculating the mean and standard deviation of the outputs. The direct statistical method and FASTA method only require two finite element solutions, one for the mean and one for the standard deviation, requiring far fewer computations and much less time than the Monte Carlo method.

The covariance matrix of the input population of 5,000 gap vectors was calculated using the direct statistical method. The middle row of this matrix is plotted as a dashed line with x-marks in Figure 5.14, compared to the middle row of the gap covariance matrix calculated from the zero-padded autocorrelation method, plotted as a solid line with circles. The two input covariance matrices are similar, and both predict very similar closure force standard deviation results, as shown previously in Figure 5.12 for the equivalent Monte Carlo simulation.

5.5 Comparison of Methods

To illustrate the differences between performing a Monte Carlo simulation versus using the FASTA method, both procedures are represented graphically in Figure 5.15.

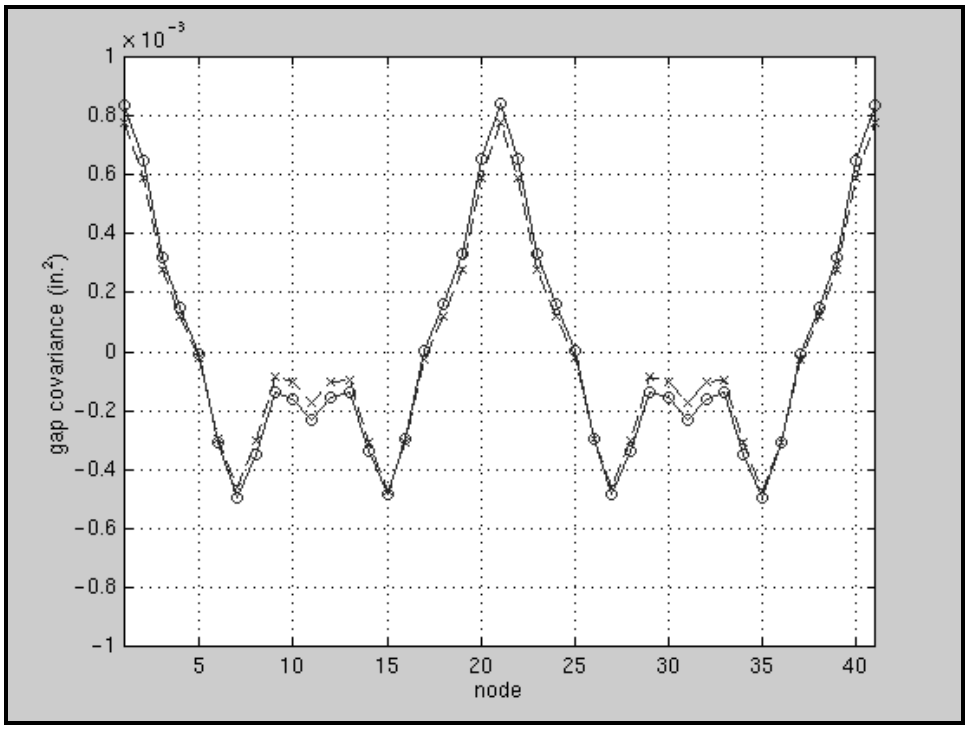

Figure 5.14 Middle row of gap covariance matrices from direct statistical method (dashed, x-marks) and zero-padded, unbiased autocorrelation (solid, circles).

The Monte Carlo method requires a simulated (or actual) sample of surface variations as input. It analyzes each of the input gap vectors, and calculates statistical descriptors of the results, such as mean and standard deviation. The FASTA method can use as input either actual surface data or a predicted frequency spectrum of the variations. It calculates the mean and covariance of the input, and performs two finite element solutions to predict the mean and standard deviation of the results.

The FASTA method assumes the covariance of two points separated by a given distance is stationary with position along the surface of each part. The geometric covariance of two points along the part surface is assumed to be a function of separation distance only, and not a function of location. Because of this, the covariance is averaged

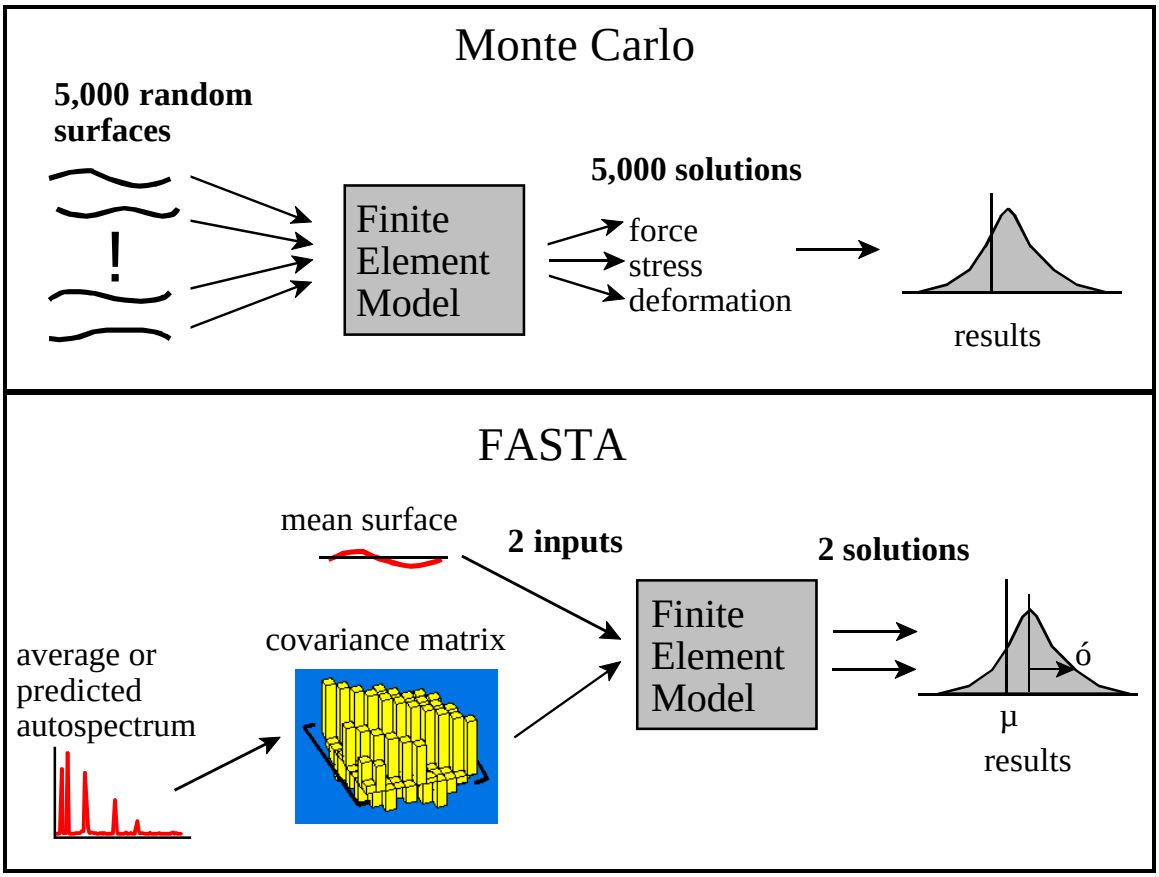

Figure 5.15 Graphical representation of Monte Carlo and FASTA procedures.

across each surface in the population to form the geometric covariance matrix. If surface variations in a population of parts truly have random phase, then the stationary process assumption is accurate, and the covariance matrix formed under this assumption will be correct. Because the FASTA method averages the surface mean and standard deviation not only across the population, but also along the surfaces, for a given sample size the results are statistically closer than other methods to an actual population, if the population has random-phase variations.

Run-times for the different methods were recorded for the 41 degree-of-freedom problem with 5,000 samples to show the increased speed of the frequency analysis

approach over the Monte Carlo method. The autocorrelation and autospectrum methods both calculated the zero-padded, unbiased autocorrelation, but the autospectrum method averaged the autospectra and then inverse transformed to get the average autocorrelation. The time required to condense the part stiffness matrices and combine them into one equivalent stiffness matrix was not included in the measured run-time. Neither was the time required to store the results in permanent memory included. The calculations were all performed on a Hewlett-Packard Visualize B180L computer using MATLAB version 5 for Unix (Kwon 1997). Run times for five different trials were averaged to account for time-share effects. One Monte Carlo simulation of 10,000 samples was also run for comparison. The run times are presented in Table 5.2 below.

Table 5.2 Average run times for force results.

Method	Average run time
Monte Carlo (10,000 FEA load cases)	12 min. 36 s.
Monte Carlo (5,000 FEA load cases)	1 min. 32 s.
Autocorrelation (2 FEA load cases, 5,000 IFFT's)	10 s.
Autospectrum (2 FEA load cases, 1 IFFT)	5 s.

Chapter 6

STATISTICAL STRESS RESULTS

In most cases, the expected range of stress caused by assembly is more useful information than predicted closure forces or deformations. Areas of high stress due to assembly can cause premature fatigue failure or even static failure if the material limits are exceeded. An airplane wing skin, for example, undergoes cyclic loading during every flight. The bottom side of the wing is in tension during flight and is very susceptible to developing fatigue cracks. If additional tensile stresses due to assembling the wing skin panels are unaccounted for, fatigue cracks may form before predicted, and perhaps be overlooked in scheduled inspection programs. Stress information is very important in the design of flexible assemblies. Again, a mean solution and a standard deviation solution will be necessary to describe the statistical distribution of assembly stress.

6.1 Mean Displacement and Stress Solutions

The preceding sections have predicted the closure force and displacements along the mating edge of two flexible parts. They have not dealt with points interior to the parts. To get internal part stresses, the displacements must be known for every degree of freedom in each part. The mean displacement solution for one part can be obtained from

the mean stiffness equation involving every degree of freedom:

$$\{\mu_F\} = [K]\{\mu_\delta\}, \tag{6.1}$$

where $\mu_{ä}$ is the vector of mean displacements, μ_F is the mean force vector, and K is the full stiffness matrix of the part. This equation is similar to Equation 3.16, except the above equation involves every degree of freedom in the part, and the stiffness matrix is not the equivalent stiffness of two mating parts.

Equation 6.1 can not be solved for the mean displacements directly, because the full stiffness matrix of a part is singular and therefore cannot be inverted. To find the mean displacements, the mean stiffness equation is separated into partitions involving known boundary displacements and unknown interior displacements, just as in Equation 3.2:

$$\begin{Bmatrix} \mu_{Fb} \\ \hdashline \mu_{Fi} \end{Bmatrix} = \left[\begin{array}{c:c} K_{bb} & K_{bi} \\ \hdashline K_{ib} & K_{ii} \end{array}\right] \begin{Bmatrix} \mu_{\delta b} \\ \hdashline \mu_{\delta i} \end{Bmatrix}. \tag{6.2}$$

In this partitioned stiffness equation, the mean displacements of boundary degrees of freedom, $\mu_{äb}$, are known, including both mating-edge and fixed degrees of freedom. The mating-edge boundary displacements are scaled from the mean gap vector using the stiffness ratio of the part:

$$\{\mu_\delta\} = [K_r]\{\mu_0\}. \tag{6.3}$$

The mean displacements of fixed boundary degrees of freedom are equal to the constrained displacement value. The mean displacements of interior (unconstrained) degrees of freedom, $\mu_{äi}$, must be found. Because a solution for the mean reaction forces,

μ_{Fb}, is not needed, only the second partitioned equation must be solved to find the interior displacements. Realizing that no forces are applied to interior nodes, the lower partition of Equation 6.2 can be rewritten as:

$$\{\mu_{Fi}\} = [K_{ib}]\{\mu_{\delta b}\} + [K_{ii}]\{\mu_{\delta i}\} = \{0\}.$$

This can be solved for the unknown mean displacements in terms of the stiffness matrix partitions and the known mean displacements, giving:

$$\{\mu_{\delta i}\} = -[K_{ii}]^{-1}[K_{ib}]\{\mu_{\delta b}\}. \tag{6.4}$$

The vector of mean displacements at every degree of freedom in the part can then be formed by mapping the interior and boundary mean displacements to one vector:

$$\{\mu_{\delta}\} = \begin{Bmatrix} \mu_{\delta b} \\ \mu_{\delta i} \end{Bmatrix}.$$

Because the reaction forces at boundary degrees of freedom are not needed, another method can be used to solve Equation 6.1 for the mean displacements. To make the stiffness matrix non-singular, each row of the stiffness matrix corresponding to a boundary degree of freedom may be set to zero, and the diagonal element of that row set to one. The known mean values of the fixed and mating-edge boundary conditions are then placed in the corresponding elements of the mean force vector. This is equivalent to setting the upper left stiffness matrix partition in Equation 6.2, K_{bb}, equal to the identity matrix, the upper right stiffness matrix partition, K_{bi}, equal to a matrix of zeros, and the mean force vector partition, μ_{Fb}, equal to the known mean displacement values. It can be seen that the upper partition of Equation 6.2 would then become simply

$$\left\{\hat{\mu}_{\delta b}\right\} = [I]\left\{\mu_{\delta b}\right\} + \{0\} = \left\{\mu_{\delta b}\right\},$$

where $\hat{\mu}_{\delta b}$ is the vector of known boundary displacements. The stiffness matrix can now be inverted to solve for the mean displacements:

$$\left\{\mu_{\delta}\right\} = [K]^{-1}\left\{\mu_{F}\right\}. \tag{6.5}$$

Equation 6.5 is still valid, because the altered rows of the stiffness matrix corresponding to boundary degrees of freedom remain unchanged when the matrix is inverted:

$$\begin{bmatrix} k & k & k & k \\ \vdots & \vdots & \vdots & \vdots \\ 0 & 0 & 1 & 0 \\ k & k & k & k \end{bmatrix}^{-1} = \begin{bmatrix} k & k & k & k \\ \vdots & \vdots & \vdots & \vdots \\ 0 & 0 & 1 & 0 \\ k & k & k & k \end{bmatrix},$$

After the boundary condition and mating-edge displacement constraints have been applied, the stiffness matrix can be inverted, and Equation 6.1 can be solved for the mean displacement vector of every degree of freedom in the part.

Once the mean nodal displacements have been found, the mean stresses can be calculated, one element at a time, using the finite element relation

$$\left\{\mu_{\sigma e}\right\} = \left[D_e\right]\left[B_e\right]\left\{\mu_{\delta e}\right\}, \tag{6.6}$$

where $\mu_{óe}$ is the element mean stress vector, and $\mu_{äe}$ is the nodal mean displacement vector for that element, extracted from the full mean displacement vector. D_e is the element constitutive matrix containing material elasticity properties, and B_e is the element kinematic matrix containing partial derivatives of the element shape functions. The

partial derivatives in B_e are typically evaluated at Gaussian quadrature points within the element, in which case $\mu_{óe}$ is the mean stresses at the Gauss points.

For finite element post-processing, nodal stresses are easiest to work with. Nodal stresses can be obtained by evaluating the B_e matrix partial derivatives at the nodal coordinates, rather than at points within the element. For 4-node quadrilateral parametric elements, a typical type of finite element, the natural coordinates of the nodes are simply (±1, ±1). The mean stress at a node is the average of the mean stress values for that node calculated from each of the connected elements. For example, if node *i* has four connected elements A, B, C, and D, as shown by node 5 in Figure 6.1, the mean stress at node *i* is the average

$$\sigma_i = \frac{1}{4}\left(\sigma_{i,A} + \sigma_{i,B} + \sigma_{i,C} + \sigma_{i,D}\right)$$

where $ó_{i,A}$ is the mean stress at node *i* calculated from element A, etc. The mean stress at each node can then be sent to a post-processor for graphical display and interpretation.

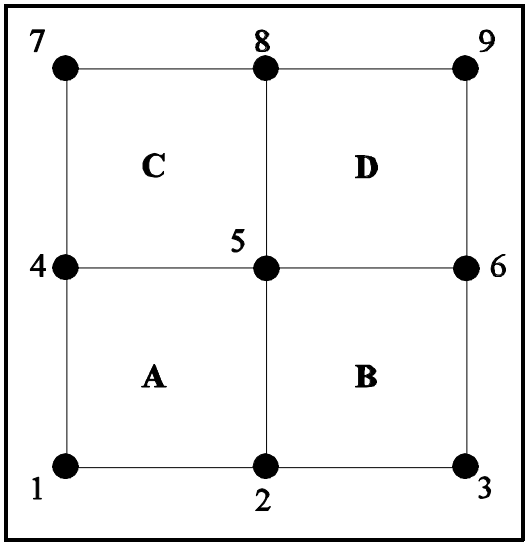

Figure 6.1 Simple 4-element part showing node and element labeling.

6.2 Full Displacement Covariance Matrix

To solve for the standard deviation of assembly stresses, a covariant solution is again needed, just as with the closure force solution in Equation 3.17. Because every degree of freedom in the part is covariant with every other degree of freedom, however, a displacement covariance matrix including *all* degrees of freedom is needed to find the stress covariance matrix and standard deviations. The displacement covariance matrix $Ó_a$, which includes covariance between all degrees of freedom, can be found from the inverse covariant stiffness equation:

$$\left[\Sigma_{\delta}\right] = [K]^{-1}\left[\Sigma_{F}\right][K]^{-1^{T}}, \tag{6.7}$$

where $Ó_F$ is the full force covariance matrix and K is the full stiffness matrix.

Again, the full stiffness matrix cannot be inverted without first applying displacement constraints for known values of fixed and mating-edge displacement covariance. The displacement covariance is zero for any covariance term involving a fixed-displacement degree of freedom, either zero or non-zero, because the displacement for that degree of freedom is constant from case to case, not random. To find the displacement covariance for mating-edge degrees of freedom, the geometric covariance matrix for the gap, $Ó_0$, must be scaled by the stiffness ratio of the part, K_r, to become $Ó_a$, the displacement covariance matrix for the part:

$$\left[\Sigma_{\delta}\right] = \left[K_r\right]\left[\Sigma_{0}\right]\left[K_r\right]^{T}. \tag{6.8}$$

In the special case of joining two identical parts, the stiffness ratio for both parts is ½ so

the mating-edge displacement covariance matrix for each part is ¼ of the geometric covariance matrix.

Although it is feasible to partition Equation 6.7 and solve for the unknown displacement covariances, solving the partitioned covariance equations is quite complicated. A simpler method for finding the displacement covariance is to set each row of the stiffness matrix corresponding to a boundary degree of freedom to zero, with a one on the diagonal term, just as in the mean displacement solution. The diagonal variance elements of the full force covariance matrix corresponding to fixed degrees of freedom are set to zero. Performing the matrix multiplications in Equation 6.7 causes $Ó_a$ to have both a zero row and column for each fixed degree of freedom. This agrees with the observation that these covariance terms are zero because they involve constrained displacements, which are constant. The geometric covariance matrix, which contains the covariance of all mating-edge displacements, is mapped to elements of $Ó_F$ which correspond to mating-edge degrees of freedom. The stiffness matrix can then be inverted, and Equation 6.7 can be solved to find the displacement covariance matrix for every degree of freedom in the part.

6.3 Stress Covariance Solution

Unlike the mean stress solution, the stress covariances and resulting standard deviations cannot be solved one element at a time. Covariance exists between all displacements, and therefore between all stresses at every node in the part. Solving the element covariant stress equation

$$\left[\Sigma_{\sigma e}\right] = \left[D_e\right]\left[B_e\right]\left[\Sigma_{\delta e}\right]\left[B_e\right]^T\left[D_e\right]^T \tag{6.9}$$

one element at a time would not account for covariance with nodes not connected to that element. As a result, covariance exists between all stress components at every node, and with all other points in the part. A stress covariance equation involving all degrees of freedom must be solved. Solving such a system is unconventional in finite element modeling, because it requires far more multiplications than solving for stresses one element at a time. Therefore, procedures do not exist for forming full kinematic or constitutive matrices involving every degree of freedom. But, if the single element stress solution is examined carefully, a full matrix equation can be written which is equivalent to solving for nodal stresses one element at a time and averaging the results.

The matrix equation for a single element stress solution is

$$\left\{\sigma_e\right\} = \left[D_e\right]\left[B_e\right]\left\{\delta_e\right\}, \tag{6.10}$$

where $ó_e$ is the element stress vector and $ä_e$ is the element nodal displacement vector. Each row of the element kinematic matrix B_e transforms nodal displacements into a particular component of strain, and each column corresponds to a particular nodal displacement. The element constitutive matrix D_e transforms these strains into stresses according to Hooke's law. The global, or full kinematic matrix B in the stress equation containing all degrees of freedom,

$$\{\sigma\} = [D][B]\{\delta\}, \tag{6.11}$$

must therefore have the same number of rows as there are total stress components for every node in the system, and the same number of columns as nodal displacements in the full system.

For a 4-node quadrilateral element, the element B_e matrix contains the shape function partial derivatives as follows:

$$\left[B_e\right] = \left[\begin{pmatrix} N^{(1)}_{,x} & 0 & 0 \\ 0 & N^{(1)}_{,y} & 0 \\ N^{(1)}_{,y} & N^{(1)}_{,x} & 0 \end{pmatrix} \begin{pmatrix} N^{(2)}_{,x} & 0 & 0 \\ 0 & N^{(2)}_{,y} & 0 \\ N^{(2)}_{,y} & N^{(2)}_{,x} & 0 \end{pmatrix} \begin{pmatrix} N^{(3)}_{,x} & 0 & 0 \\ 0 & N^{(3)}_{,y} & 0 \\ N^{(3)}_{,y} & N^{(3)}_{,x} & 0 \end{pmatrix} \begin{pmatrix} N^{(4)}_{,x} & 0 & 0 \\ 0 & N^{(4)}_{,y} & 0 \\ N^{(4)}_{,y} & N^{(4)}_{,x} & 0 \end{pmatrix}\right]_P ,$$

where $N^{(1)}_{,x}$ is the partial derivative of the first shape function with respect to the *x* direction, $N^{(1)}_{,y}$ is the derivative of the first shape function with respect to *y*, etc., and all derivatives are evaluated at a node or point P within the element. Because the stresses in any element are only a function of the displacements of nodes connected to that element, the columns of the element kinematic matrix may be separated and mapped onto the corresponding columns of the global kinematic matrix, with zeros placed in the other columns. The rows of each column remain grouped together because they represent strain components at the same node, which is how the global stress vector is ordered:

$$\{\sigma\} = \left\{\begin{pmatrix} \sigma_{x,1} & \sigma_{y,1} & \tau_{xy,1} \end{pmatrix} \quad \begin{pmatrix} \sigma_{x,2} & \sigma_{y,2} & \tau_{xy,2} \end{pmatrix} \quad \cdots \right\}^T .$$

Because the displacements of each node are also grouped together in the global displacement vector, the submatrices of B_e, relating displacements at the same node to strains at the same node (3 by 3 submatrices for the 4-node quadrilateral element shown above), can be mapped as submatrices to the global B matrix. This mapping is performed

for every connected node of the element, evaluating the partial derivatives in B_e at the proper node each time.

If a node is connected to more than one element, the columns of the element matrix are added to those which have already been mapped to the global matrix from previous elements. When this is completed, each row of the global B matrix is divided by the number of elements connected to that node, which causes the nodal stresses calculated in the global stress equation

$$\{\sigma\} = [D][B]\{\delta\}$$

to be averages of the nodal stresses predicted by each connected element, just as they were averaged when solving for stresses one element at a time. Figure 6.2 depicts this mapping for the simple 4-element part of Figure 6.1. In Figure 6.2, B_i are the kinematic matrices for elements A, B, C, and D, and $\left(N^{(1)}_{,x}\Big|_1 \right)_A$ is the partial derivative of the first shape function of element A with respect to the x direction, evaluated at node one, $\left(N^{(1)}_{,y}\Big|_2 \right)_B$ is the partial derivative of the first shape function of element B with respect to the y direction, evaluated at node two, etc. The constitutive matrix of material properties must also be expanded to a global matrix, one relating all strains in the system to stresses.

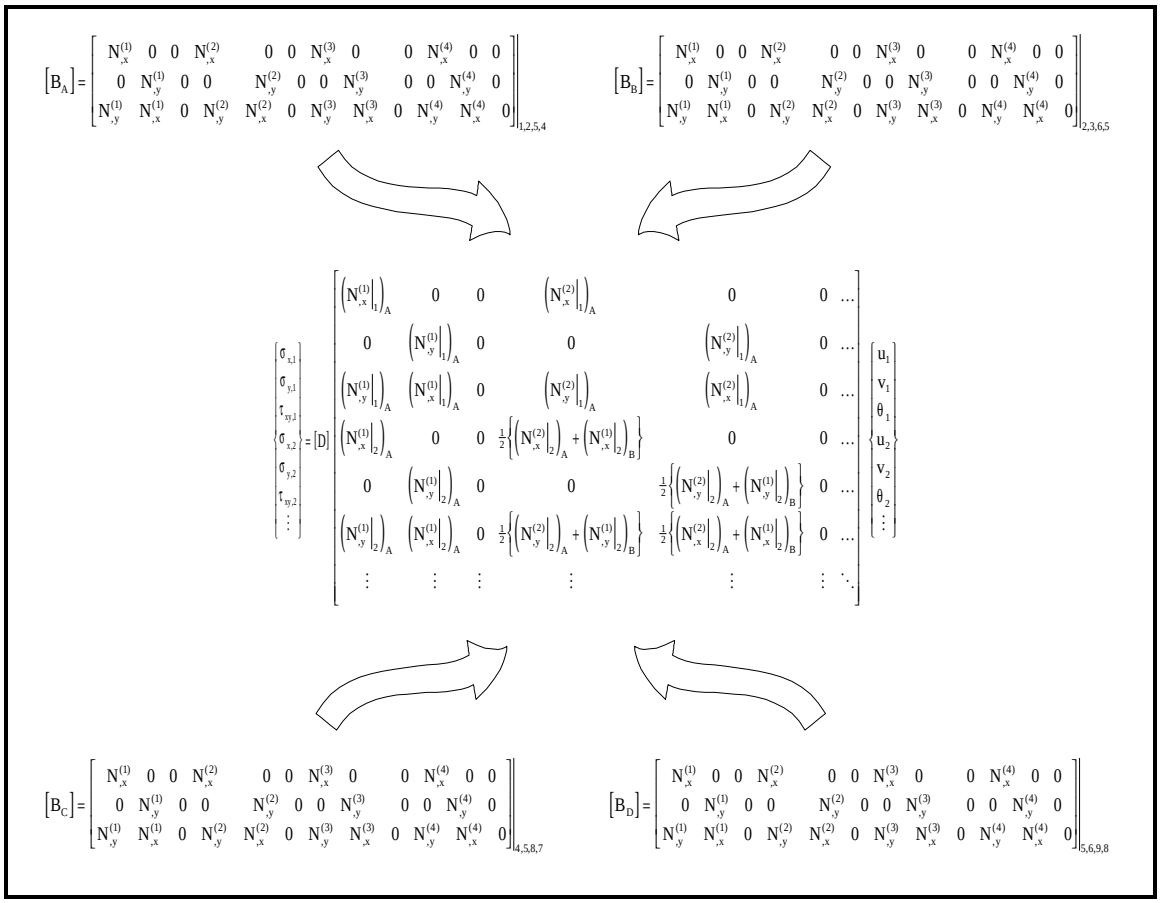

Figure 6.2 Mapping element kinematic matrices to global kinematic matrix.

For a plane-stress element, also used for bending stresses in plate elements, the element constitutive matrix is:

$$\left[D_e\right] = \frac{E}{1-\nu^2}\begin{bmatrix} 1 & \nu & 0 \\ \nu & 1 & 0 \\ 0 & 0 & \frac{1-\nu}{2} \end{bmatrix},$$

where E is the material's elastic modulus and í is Poisson's ratio for the material. In the element stress equation, Equation 6.7:

$$\left\{\sigma_e\right\} = \left[D_e\right]\left[B_e\right]\left\{\delta_e\right\},$$

the D_e matrix relates strains at a node to stresses at that node, and is the same for every element of the same material. The state of stress at any node depends only on the strains at that node. Because of this, the element constitutive matrix can be mapped to a global constitutive matrix by simply placing it in the diagonal submatrices of the global D matrix, with all other terms zero. This creates a global D matrix which relates strains at each node in the system to stresses at that node.

Once the displacement covariance, kinematic, and constitutive matrices have been formed which include every degree of freedom in the part, the global covariant stress equation

$$\left[\Sigma_{\sigma}\right] = [D][B]\left[\Sigma_{\delta}\right][B]^{T}[D]^{T} \tag{6.12}$$

can be solved for the stress covariance at every node in the system, where $Ó_ó$ is the global stress covariance matrix, and $Ó_á$ is the global displacement covariance matrix found earlier. The standard deviation of each stress component at all nodes can be found by taking the square root of the stress variance, the diagonal terms of the stress covariance matrix $G_ó$. Knowing this, and the mean stresses at each node, the probable range of stresses due to assembly can be predicted at each node within the part. The mean and standard deviation stress levels can be plotted with any post-processor for graphical interpretation.

Chapter 7

VERIFICATION OF STRESS RESULTS

To verify the FASTA method for predicting the range of stresses caused by assembly, the lap joint problem shown in Figure 3.2 was again analyzed by the frequency analysis method, using the global covariant stress equation, and the results compared with a Monte Carlo simulation. The parts were meshed into a 10 by 10 grid of bending-only plate elements. Because the parts are thin, the plane stress assumption was used and stress normal to the plates was assumed to be negligible. This left three in-plane stress components, $\acute{o}_x$, $\acute{o}_y$, and $\hat{o}_{xy}$, and two transverse shear stress components, $\hat{o}_{xz}$ and $\hat{o}_{yz}$. The same simulated population of 5,000 gaps that was used for verification of closure force results in Chapter 5 was used as input for both methods. These gaps contained both random and non-random variations. Because a coarser mesh was used for the stress solutions, the gaps were re-sampled at every fourth data point to create gap vectors containing only 11 nodal variations. The FASTA method used the mean displacement and displacement covariance to predict the statistical stress distribution, while the Monte Carlo simulation calculated the stress for all 5,000 sample assemblies.

7.1 Frequency Analysis Method

The frequency content of the simulated population of gaps was used to predict assembly stresses when the two parts were fastened together. Two finite element solutions of each part were required, one to predict the mean assembly stresses and one to predict the stress covariance. The mean displacement vector for both parts was calculated from the mean gap vector using the stiffness ratio of each part, which was ½ for each part in this assembly (Equations 3.12 and 6.3). The mean displacement vector was applied as a boundary condition along the mating edge of one part, and the mean displacements throughout the entire part were found. The mean assembly stress vector was then calculated for every node in the part using the global stress equation,

$$\{\mu_\sigma\} = [D][B]\{\mu_\delta\},$$

where μ_σ and μ_δ are the mean stress and mean displacement vectors for every node in the part. The contour plot in Figure 7.1 shows the predicted mean assembly stresses in the direction of the mating edge (x-direction). The plot looks down from above the part, with the mating edge at the bottom of the picture and the fixed edge at the top. The mean stresses are due to the deterministic variations with non-random phase included in the simulated population of gaps. If no deterministic surface variations are present, the mean assembly stresses will be zero.

The average autocorrelation of the simulated gap vectors was used to approximate the geometric covariance matrix, which was scaled by the stiffness ratios to form the displacement covariance matrix for each part. The full displacement covariance matrix was found for one part, as in Equation 6.6. The stress covariance matrix was calculated,

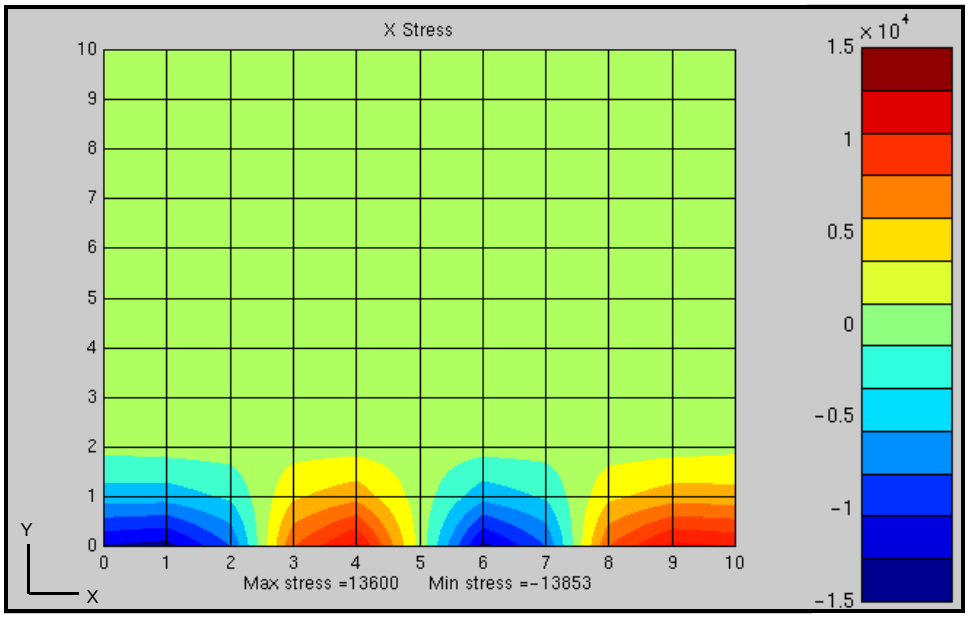

Figure 7.1 Mean assembly normal stress in x-direction.

containing covariance between all five stress components at every node in the part, from Equation 6.11. The standard deviation of assembly stress was given by the square root of the variance terms in the stress covariance matrix. The standard deviation of x-direction normal stress throughout the part is shown as a contour plot in Figure 7.2. The variation in stress is fairly uniform along the mating edge, with peak stress variation occurring at the corners. The standard deviation of normal stress in the x-direction along the mating edge is plotted in Figure 7.3 to show the variation in assembly stress from part to part due to surface irregularities. It is significant to notice that for this population of gaps, the magnitudes of assembly stress variation are approximately three times larger than are the mean assembly stresses. Knowledge of such large variations in stress could be critical in designing assemblies.

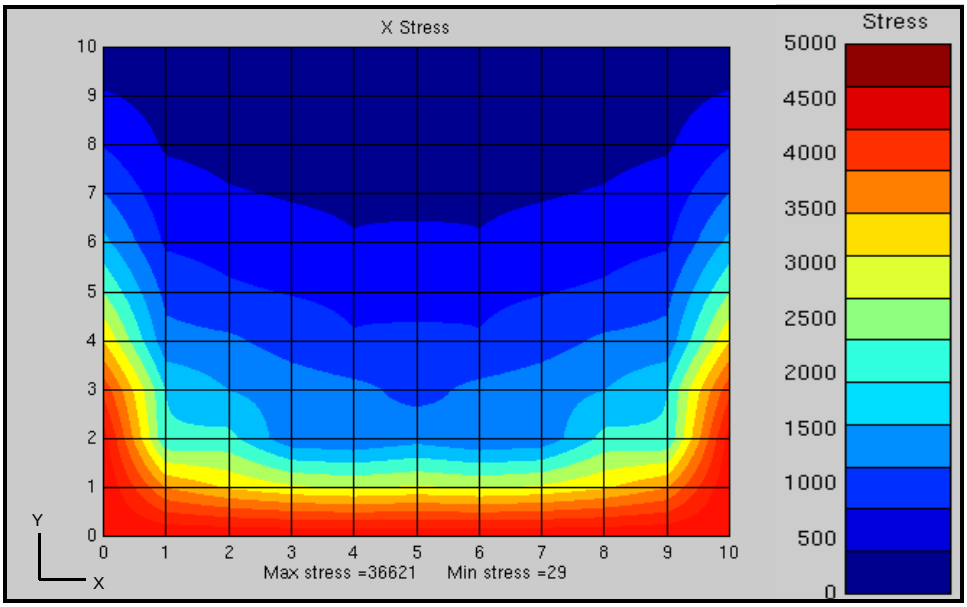

Figure 7.2 Standard deviation of assembly normal stress in x-direction from FASTA method.

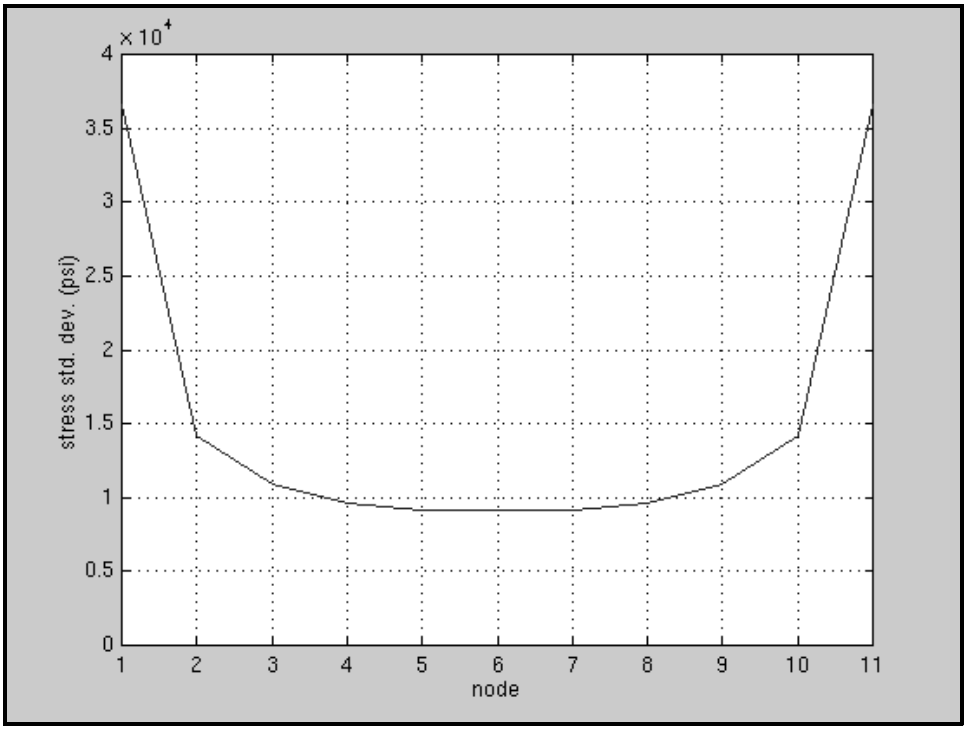

Figure 7.3 Standard deviation of assembly normal stress in x-direction along mating edge from FASTA method.

7.2 Monte Carlo Simulation

For comparison, the assembly stress distribution was also predicted using a Monte Carlo simulation. Unlike the FASTA method, which calculated a single mean gap vector and gap covariance matrix as input, the Monte Carlo method calculated the stresses for each of the 5,000 simulated assemblies one at a time. The Monte Carlo method was also used to further verify Equations 6.11 and 6.12, the global stress equations, and the global kinematic and material properties matrices, as explained in Section 6.3. The Monte Carlo method used bilinear extrapolation to calculate nodal stresses from the Gauss point stresses element by element, averaging to predict the stress at nodes connected to more than one element. The nodal stress data for the 5,000 cases was accumulated, and the mean stress vector and stress covariance matrix were calculated statistically from this data. The standard deviation of assembly normal stress throughout the part in the x-direction is plotted in the contour plot of Figure 7.4. Figure 7.5 is a plot of these stresses along the mating edge, shown as a solid line. For comparison, the standard deviation of normal stress along the mating edge predicted by the FASTA method is re-plotted as a dashed line. The two methods gave extremely similar results. The difference is caused by the additional averaging of geometric covariances along each surface in the FASTA method, which gives a closer approximation to the covariance of the population. Again, the FASTA method was much faster, requiring only two finite element analyses versus 5,000 for the Monte Carlo method, but gave the same results.

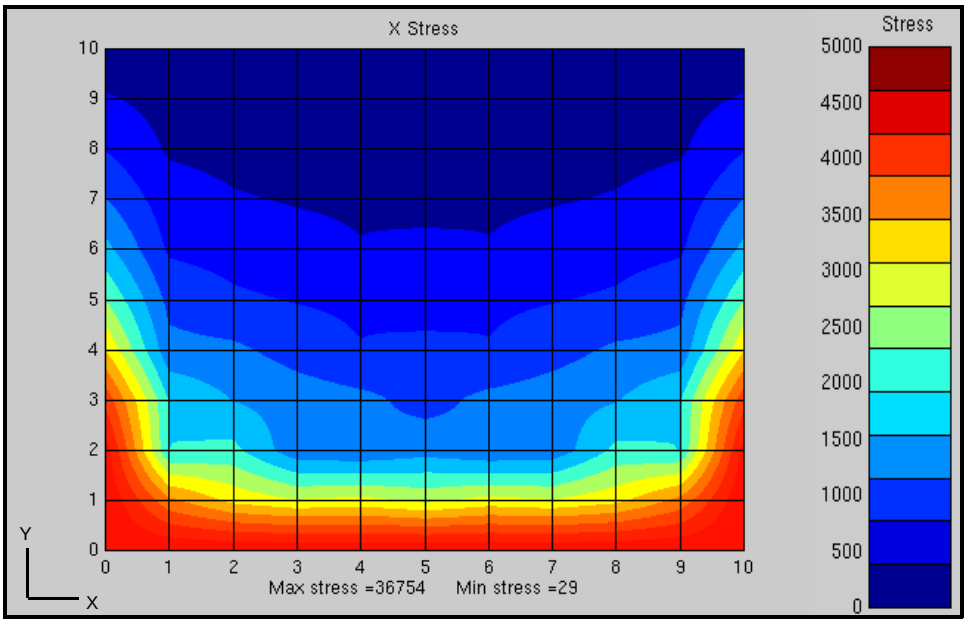

Figure 7.4 Standard deviation of assembly normal stress in x-direction from Monte Carlo.

Because stress solutions require a much longer time to compute than force results,

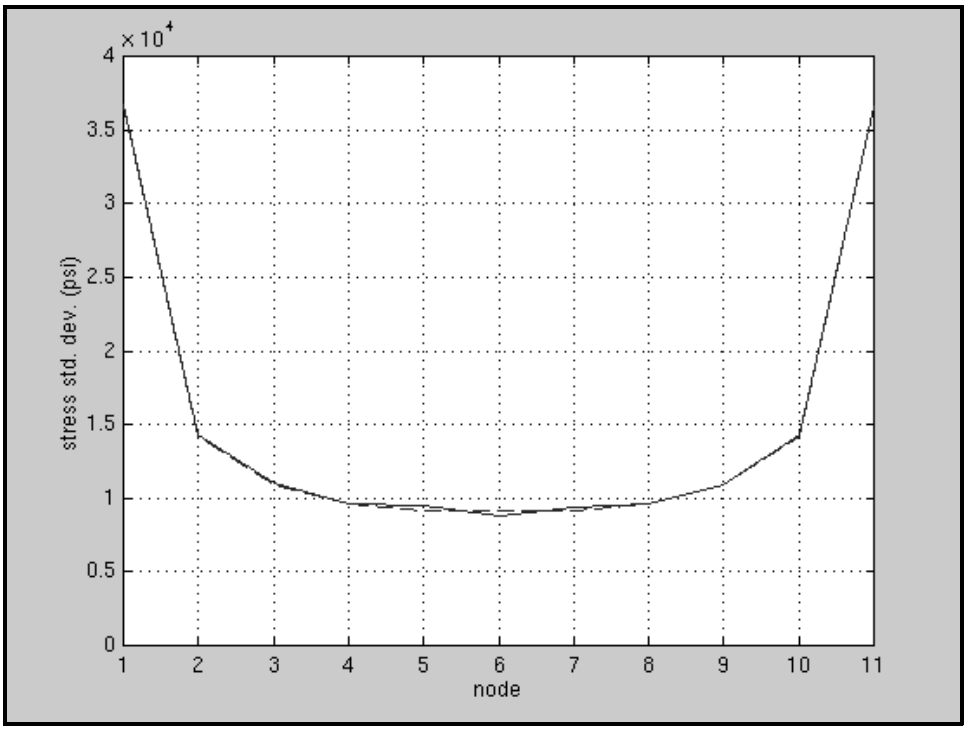

Figure 7.5 Standard deviation of assembly normal stress in x-direction along mating edge from Monte Carlo (solid) and FASTA method (dashed).

the time saved using the FASTA method versus a Monte Carlo simulation is even greater when predicting assembly stresses. The time required to calculate the mean and covariance stress results, presented above, for the same population of 5,000 input gap vectors was recorded for both a Monte Carlo simulation and a FASTA method analysis. The calculations were all performed on a Hewlett-Packard Visualize C240 computer using MATLAB version 5 for Unix (Kwon 1997). Because of the length of time involved, only one Monte Carlo simulation was performed. The run time for five FASTA method analyses were averaged to account for time-sharing effects. The computation times are recorded below in Table 7.1.

Table 7.1 Average run times for stress results.

Method	Average run time
Monte Carlo (5,000 FEA load cases)	3 hr. 15 min. 12 s.
FASTA (2 FEA load cases)	0 min. 13 s.

In predicting stress results, the FASTA method is extremely faster than a Monte Carlo simulation of the same input population, and gives nearly equivalent results. And, Monte Carlo simulations require a larger sample size for equivalent accuracy due to the averaging of covariances that occurs in the FASTA method.

Chapter 8

WAVELENGTH SENSITIVITY OF ASSEMBLY RESULTS

One advantage of using spectral analysis to model surface variations in flexible assemblies is the capability of investigating the effect of the frequency content of those variations. The gap covariance matrix includes the combined effect of all wavelengths of variation, so the contribution of any particular wavelength to assembly results is lost. To illustrate the effect of variation wavelength on predicted assembly stress results, the FASTA method was used to predict the range of assembly stresses from surfaces containing only a single wavelength of variation. Four cases were analyzed, each with a different variation wavelength. The stress results showed high sensitivity to the wavelength of surface variation.

Returning to the simple lap joint assembly of previous examples, a population of single-wavelength gap vectors was created and used as input into the model. As before, two flat plates fastened by a lap joint were meshed into a 10 by 10 grid of bending-only plate elements, and gap vectors formed which describe the vertical displacement of mating-edge nodes. All gap vectors used in this simulation have an amplitude of 0.10 inches and uniformly-random phase distributions. The four wavelengths of variation are non-dimensionalized by using the ratio of variation wavelength to the characteristic length

(C.L.) of the surface (Anderson 1997). In this case, the characteristic length of each surface is the edge length of the parts, 10 inches.

8.1 Discretized Uniform Phase Distribution

Because the gap vectors in this simulation had only a single wavelength, and because they are discrete processes, only discrete phase shifts are necessary to accurately and completely model a uniform random phase distribution. Rather than generate a large number of random phase shifts, a series of equally-spaced phase shifts was used. The phase shift step size was equal to the node spacing interval along the mating edge, from 0 to 2ð. This can be written mathematically as

$$\phi_i = \left(\frac{i}{n-1} \right) 2\pi, \qquad i = 1 \text{ to } n\text{-}1, \tag{8.1}$$

where there are n nodes along the mating edge, and ϕ_i is the phase shift for the i^{th} single-wavelength gap vector. If the gap vectors have multiple wavelengths, every possible combination of wavelength and phase shift must be included in the population, and the problem is increased in size exponentially. However, accurate results are obtained for single-wavelength variations by representing a uniform phase distribution as a series of discrete phase shifts, requiring a much smaller population of gap vectors than if the phase shifts are randomly generated.

To test this approach of using discretized phase distributions, a population of gap vectors was created which contained 50,000 sinusoidal gaps with uniformly random phase, and wavelength equal to the characteristic length. The direct statistical method was used

to calculate the gap covariance matrix and predict the closure force standard deviation along the mating edges of the two parts. Another population of only 10 single-wavelength gaps was created with discrete phase shifts representing a uniform phase distribution. The closure force standard deviation was predicted for this population using the FASTA method. Results from the two populations are plotted together in Figure 8.1. Closure forces along the mating edge predicted by the direct method from the 50,000-gap population are plotted as a solid line, while closure forces predicted by the FASTA method from the 10-gap population are plotted as circles. Results from the two different populations match exactly, showing that a uniform phase distribution can be represented by only a few discrete phase shifts.

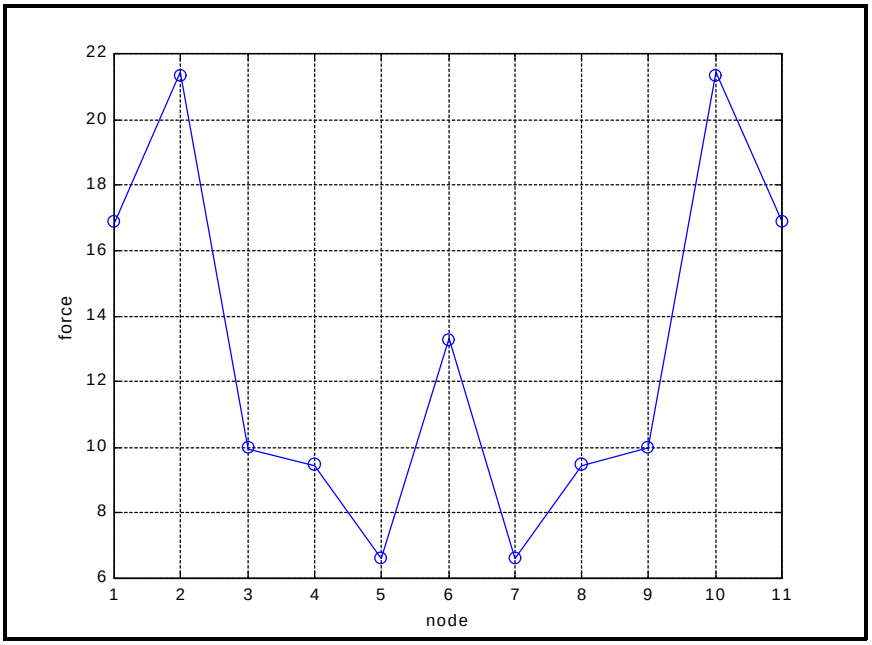

Figure 8.1 Closure force standard deviation along mating edge from direct (solid) and FASTA (circles) methods.

8.2 Stress Results

The FASTA method was used to predict the covariant assembly stress results for populations of 10 surface variation vectors with discretized uniform phase distributions, and wavelength to characteristic length ratios equal to 1, ½ a, and ¼. All gaps consisted of single-wavelength sinusoids with amplitude equal to 0.010. In this case, the variations along single part surfaces were simulated, rather than the gap vectors between parts. From these surface variation vectors, a mean variation vector and a displacement covariance vector were calculated using the zero-padded, un-biased autocorrelation function. The mean stress solution, full displacement covariance matrix, and stress covariance matrix were calculated as explained in Chapter 6.

Because the mean variation of each surface in each population was zero, the mean assembly stresses for all four cases were zero. The standard deviation of normal stress results for these four cases, in the x-direction, are plotted in Figures 8.2 through 8.5 below. The same stress color map was used for all standard deviation stress contour plots to better compare the predicted variation in assembly stresses. To avoid aliasing, variations with wavelengths shorter than 1/5 the characteristic length can not be correctly modeled because the edge of the part is only meshed into 10 elements whose length is 1/10 of the characteristic length. But, the frequencies tested are sufficient to show trends in how the wavelength of surface variation affects assembly stress results.

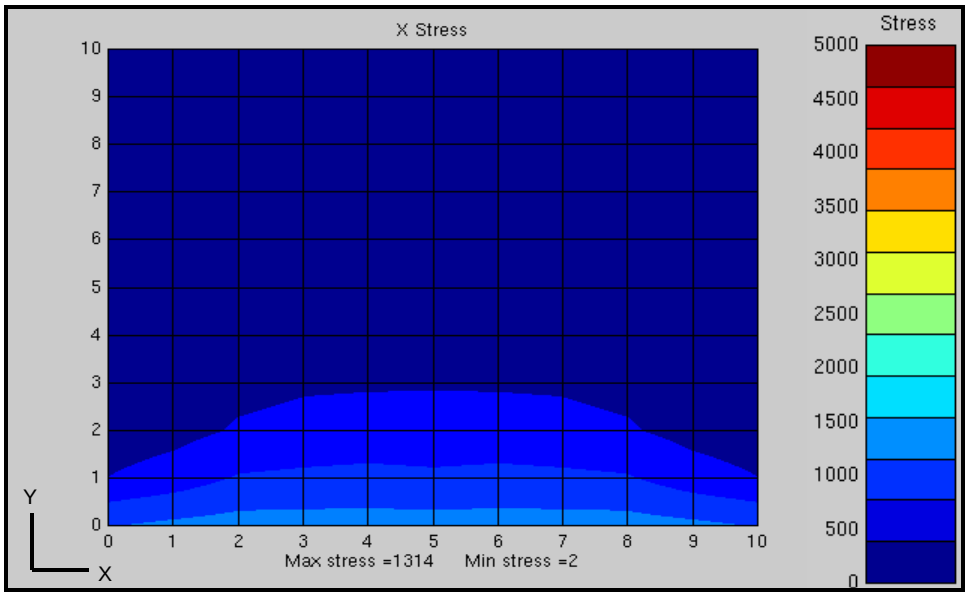

Figure 8.2 Standard deviation of normal stress in the x-direction, wavelength/characteristic length ratio = 1.

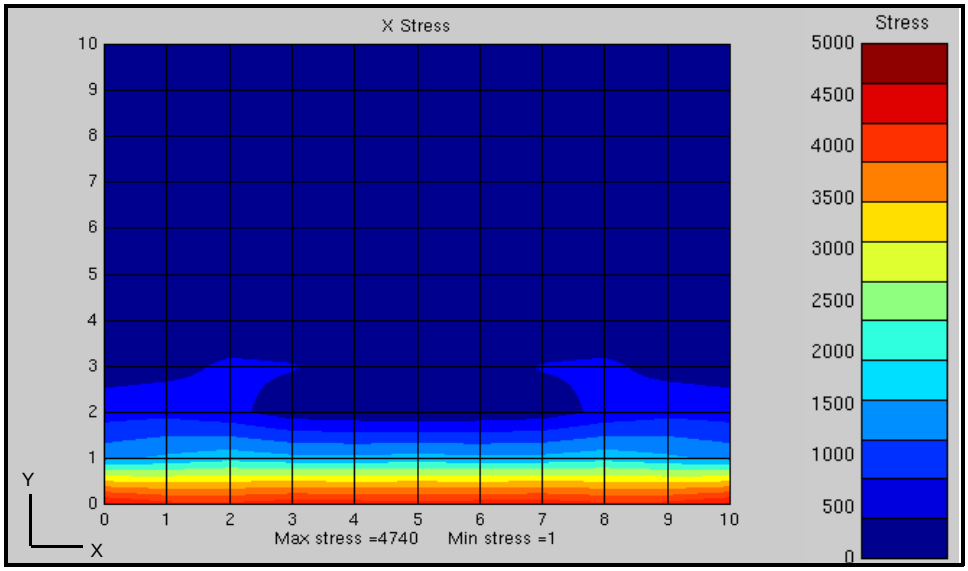

Figure 8.3 Standard deviation of normal stress in the x-direction, wavelength/characteristic length ratio = 1/2.

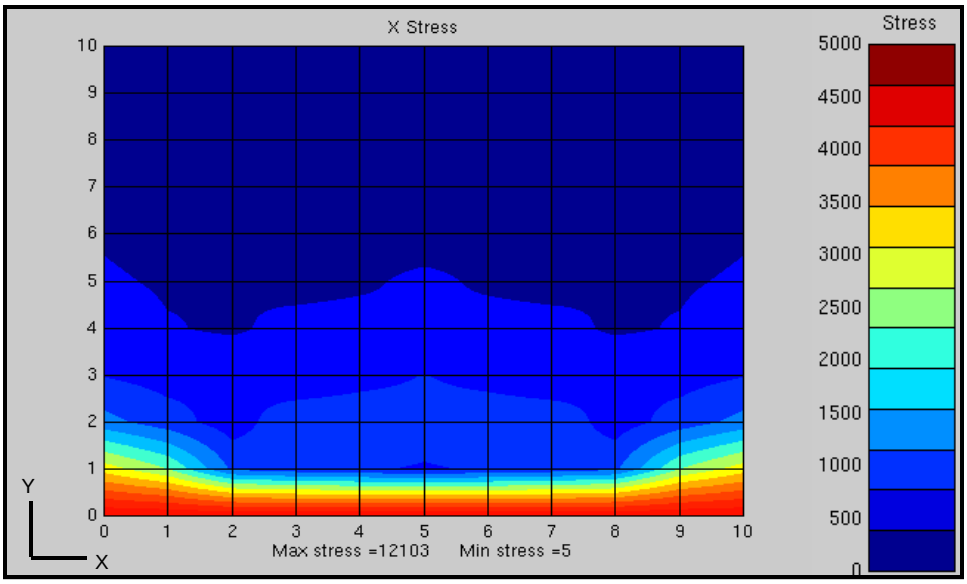

Figure 8.4 Standard deviation of normal stress in the x-direction, wavelength/characteristic length ratio = 1/3.

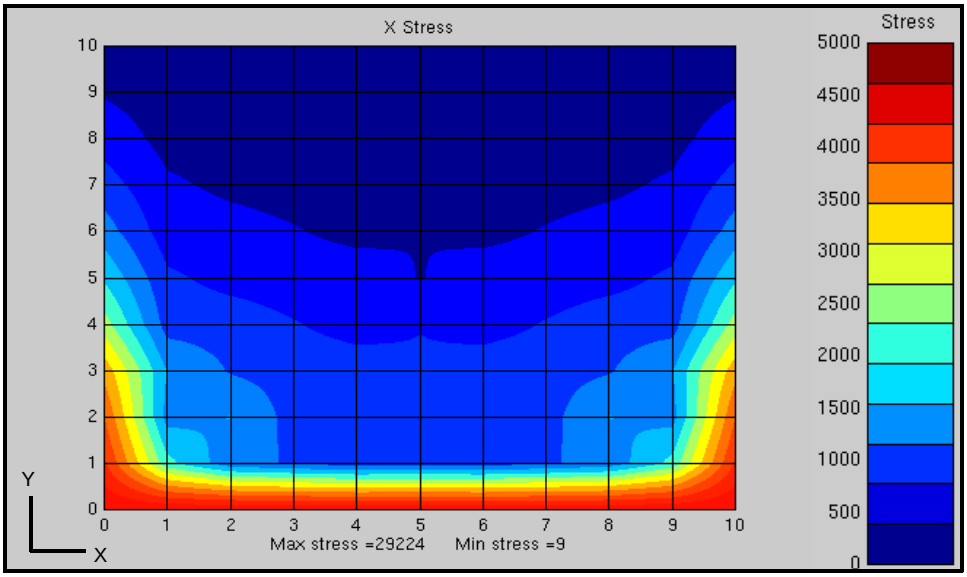

Figure 8.5 Standard deviation of normal stress in the x-direction, wavelength/characteristic length ratio = 1/4.

8.3 Wavelength Sensitivity

Several trends can be seen in the above figures. The areas of probable high stress due to assembly do not propagate into the part as far for shorter-wavelength variations. Surfaces containing short-wavelength variations will cause higher local assembly stresses, but these stresses will not propagate into the parts very far. Also, assembly stresses from surfaces with short-wavelength variation are concentrated more at the ends of the mating edge. Explicit relationships for these trends are needed for use in tolerance allocation, and should be derived in future work.

To show the effect of decreasing wavelength (increasing frequency) on assembly stresses, the peak normal stress standard deviation from each of the four cases analyzed above is plotted as a solid line in Figure 8.6. The dashed line represents the average standard deviation of x-direction normal stress along the mating edge for each of the four cases. The plot shows a rapid increase in the sensitivity of assembly stress variance to variation frequency as the wavelength of surface variations decreases. Again, specific relationships for this sensitivity are needed for use in tolerance allocation.

Looking at Figure 8.6, it appears that not including variations with wavelength less than twice the nodal spacing in an assembly model would cause significant errors in the predicted assembly results. However, even though the predicted standard deviation of assembly stress increases rapidly for shorter variation wavelengths, this comparison used variations which all had the same amplitude. In actuality, the relative amplitude of surface

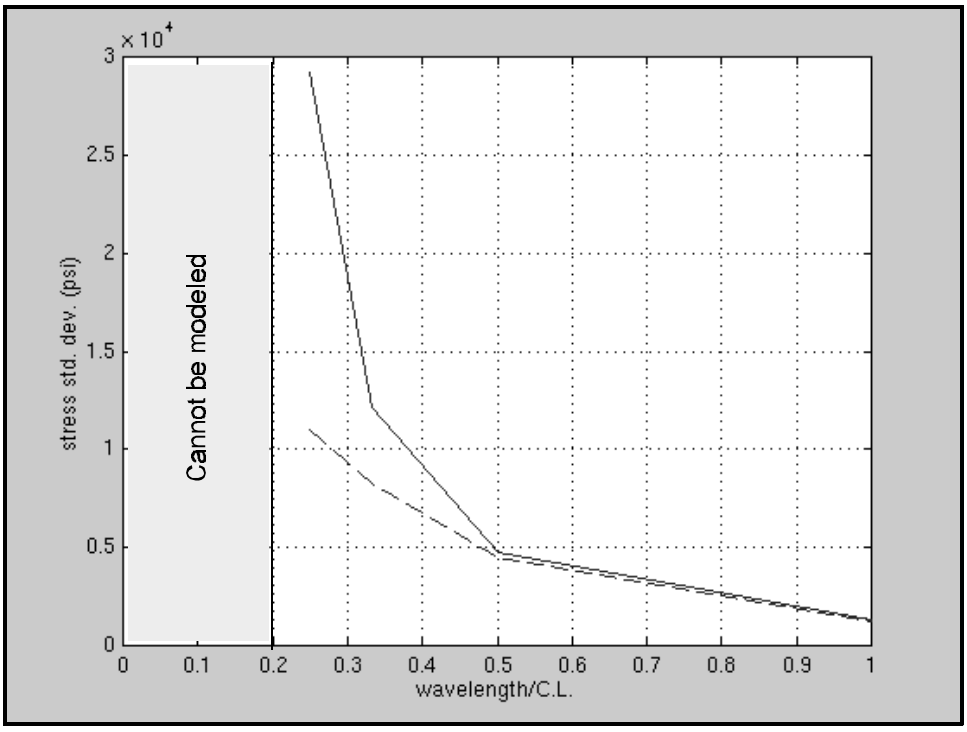

Figure 8.6 Standard deviation of normal stress in the x-direction along the mating edge versus variation wavelength, peak (solid) and average (dashed).

variations decreases rapidly for shorter wavelengths. This fact allows selecting a cutoff wavelength, below which shorter variations need not be included in the assembly model.

Chapter 9

DISCUSSION OF RESULTS

Statistical tolerance analysis is useful both in predicting variations from assembling a population of existing parts, and in designing and tolerancing parts prior to production to ensure that they will function properly when assembled. This chapter discusses several issues involved in predicting results for assemblies of flexible parts. It also discusses the application of spectral surface tolerances and finite element analysis to the design of flexible assemblies.

9.1 Measured Surface Variation Data

If sufficient surface variation data is available to represent a population of parts, the fastest method for predicting assembly results is to calculate the covariance matrix of the surface variations directly. Using the statistical definition, the covariance matrix of sampled surface variation data is calculated and used as input into the statistical finite element model. This method gives identical results to Monte Carlo simulations, regardless of sample size, since the covariance matrix is derived from the same set of input surfaces. This is because a linear finite element model is used to model the flexible assembly.

If limited surface data exists for a population, the FASTA method presented in this

paper can be used to predict assembly results more accurately than Monte Carlo or direct statistical methods, if the covariance of the random surface variations is stationary. Because the covariance of surface variations is assumed to be stationary, the FASTA method averages the covariance not only through the population of parts, but also along the part surfaces. The covariance predicted by the autocorrelation function in the FASTA method is the average of the covariance at all points along the surface. The FASTA method assumes that the covariance at every node along the mating surface is equal to the average covariance. This is true if the random surface variations have a uniform phase distribution, and if the frequency content of the random variations does not change along the surface. Measured part data can be analyzed for stationarity to justify these assumptions.

9.2 Effect of Frequency Aliasing and Leakage

Because surface variations are modeled as discrete processes having values only at finite element nodes, the surface is in effect sampled at a rate equal to the nodal spacing. If the nodal spacing along mating surfaces of the finite element assembly model does not correspond to the spacing of measured data points, some interpolation error will occur in predicting the surface variation at finite element nodes between data points. This interpolation error can be attributed to frequency aliasing and leakage.

Frequency aliasing arises from sampling surface variations which contain wavelengths which are shorter than twice the nodal spacing. When sampled, shorter wavelengths are aliased, or appear as longer wavelengths than they actually are. This can

be seen in Figure 9.1 where a process, represented by a solid line, has been sampled using a frequency which is too low. The sample points, shown as circles, appear to lie on a wave of longer wavelength, represented by a dashed line.

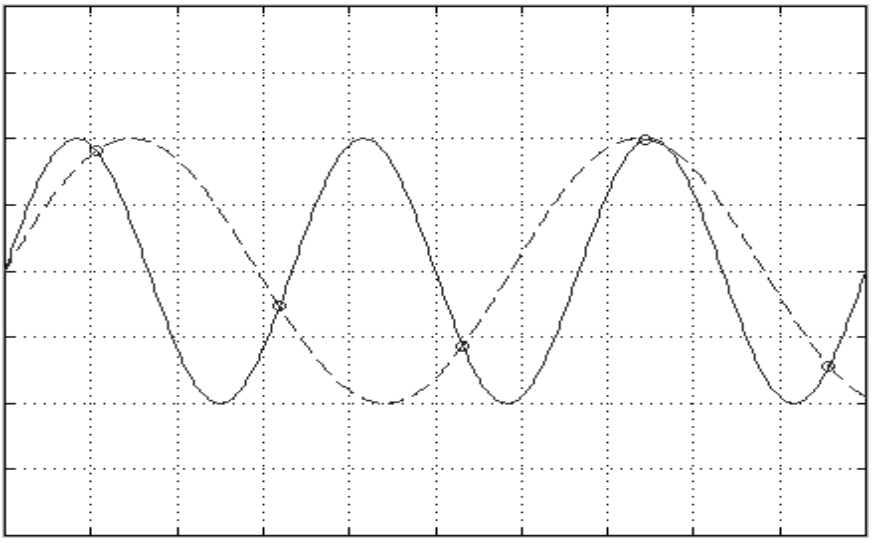

Figure 9.1 Frequency aliasing from sampling with too low a frequency.

Frequency aliasing does not add error at known data points in either the spatial or frequency domain, but does introduce error when interpolating values between known data points. If finite element nodes are not aligned with the location of known data points, surface variations with wavelengths which are shorter than twice the nodal spacing cannot be included in the model without introducing error due to frequency aliasing.

Frequency leakage arises from assuming a sampled process is periodic inside the sample length. This is caused by discretizing the frequency spectrum. Only wavelengths which are evenly divisible into the sample length are included in the discrete spectrum. Other frequencies between these discrete values are “leaked” to surrounding discrete frequencies. Superimposing these discrete frequencies will, however, exactly reproduce

the original data points. As with aliasing, error occurs only when interpolating points between known data points. Because the value of surface variation is only needed at nodal locations, leakage does not introduce any error if the finite element nodes have the same spacing as sampled data points. If nodal locations do not coincide with the locations of measured data, frequency leakage will introduce error into the model.

9.3 Effect of Surface Sampling Rate

One method for accurately modeling a part surface is to first measure the surface variations using a high sample rate and transform this data into the frequency domain using the FFT. The frequency content of the surface can be examined and used to choose an upper frequency limit, above which the amplitude of surface variations are not significant and can be excluded from the model. If the upper frequency limit is 1/n of the cutoff frequency associated with the data sampling rate, where n is an integer, then a node can be created in the finite element model corresponding to every n^{th} data point. If the ratio between the upper frequency limit and the cutoff frequency of the sampling rate is not an integer, the sampled data may be used to interpolate surface variation values for finite element nodes between known data points. This will introduce some error associated with frequency aliasing and leakage. If these errors are not acceptable, the surface must be measured again using a sampling frequency which is an integer multiple of the upper frequency limit for the model.

Frequency aliasing and leakage may also produce error in measured data when sampling surface variations. Sampling techniques and part measurement are beyond the scope of this paper.

9.4 Designing with Spectral Analysis

The FASTA method can be used to predict forces, distortions, and stresses which may affect the functionality of flexible assemblies. This can be done prior to production, based on the expected surface variations of mating parts. The FASTA method can also help in specifying tolerances on surface variations by predicting the sensitivity of assembly results to different variational wavelengths.

After the nominal shape of flexible parts to be assembled has been defined, surface variation tolerances may be placed on critical mating surfaces. Tolerances for rigid parts are commonly specified by defining allowable bounds on the surface. But this is not sufficient to control deformations and stresses in assemblies of flexible parts. As has been shown, both the frequency and amplitude of surface variations affect flexible assembly results. Surface tolerances for flexible parts should include the allowable wavelength and amplitude content of the surfaces, in the form of an allowable surface variation frequency spectrum. Assembly results can be predicted from these tolerances. A worst-case analysis can be performed by assuming that all surface variations are at the limit of their spectral tolerance. Or, a statistical analysis may be performed if the average and standard deviation of allowable surface variation spectra can be defined.

If information is available about the manufacturing processes to be used, the designer can predict the expected wavelengths and amplitudes of variation due to a particular process. If non-random variation is expected, such as part warping, this could also be estimated. Such information would then be used to create the expected mean gap vector, autocorrelation sequence, and gap covariance matrix for the assembly. These would be used in predicting the expected range of assembly forces, deformations, and stresses, and in estimating the predicted fraction of rejects.

Once a finite element model of an assembly has been created, it can be used to analyze any number of misalignment and surface variation cases by simply changing the mean gap vector and geometric covariance matrix and repeating the FEA calculations. This is similar to analyzing different load cases in conventional finite element analyses. Neither the individual part stiffness matrices, the combined and condensed (super-element) stiffness matrices, the kinematic matrices, nor the constitutive matrices need to be recalculated for different cases of misalignment or surface variation.

9.5 Tolerance Allocation

The FASTA method could be implemented in a tolerance allocation algorithm in which the lowest-cost arrangement of surface tolerances is found which still meets assembly requirements, such as closure force, deformation, and stress limits. This would require explicit knowledge of the sensitivity of assembly results to different wavelengths of surface variation, as well as manufacturing process capabilities. One method may be to analyze single-wavelength variations one at a time to study the contribution of each

variational wavelength to the total assembly results. The sensitivity could be described as the ratio between the amplitude of surface variation and the amplitude of assembly results, as a function of variation wavelength. Tolerance allocation for flexible assemblies using spectral analysis should be the subject of future research.

Chapter 10

CONCLUSIONS AND RECOMMENDATIONS

Flexible assembly tolerance analysis can predict the probable range of assembly results when compliant parts are joined to form an assembly by accounting for part flexibility as well as surface variations. Tolerance analysis of flexible assemblies can predict assembly results not possible with other tolerance analysis methods, such as forces required for closure of gaps, internal stresses, and part deformations.

10.1 Conclusions

Assemblies of flexible parts can be modeled using finite element analysis, with aligning nodes forced together along mating surfaces. Statistical tolerance analysis of flexible assemblies must account for covariance of displacements and variations between finite element nodes along the mating part surfaces. This covariance affects the predicted range of deformation, closure force, and stress due to assembly. The covariance of surface variations is described in the FASTA method by modeling surface variations of flexible parts in the frequency domain. Assembly results predicted by the FASTA method agree with results from Monte Carlo simulations and with results from calculating the covariance matrix of the surfaces directly from the statistical definition.

Using the frequency spectrum method for flexible assembly tolerance analysis, engineers can measure surface variations of existing parts and predict the statistical distribution of assembly forces, stresses, and distortions. They can also use it to find the allowable surface variation of flexible parts, given an acceptable level of assembly stress and deformation. Representing surface variations in the frequency domain aids in locating and reducing sources of variation in the manufacturing process. Deterministic, or bias variations, and random variations can be analyzed and controlled separately. Representing surface variations with a frequency spectrum relates well to the definitions of surface roughness, waviness, and form variation outlined in the ASME Y14.5.1M - 199x standard.

10.2 Contributions

The following significant contributions were made to statistical tolerance analysis of flexible assemblies:

1. A comprehensive system was developed for statistically predicting results from assembling flexible parts having surface variations, combining concepts from Statistical Tolerance Analysis, Finite Element Analysis, and Spectral Analysis. The system accounts for surface variation and surface waviness. The system requires only two finite element solutions to predict the mean and standard deviation of part deformation and assembly closure force.

a. The system models surface variations using discrete Fourier series. This allows direct determination of the effect of specific variational wavelengths on assembly results.

b. An appropriate method was demonstrated for using the average autospectrum of surface variations to approximate the geometric covariance matrix for of a population of surfaces. The method accounts for the finite length of part surfaces by padding surface variation data with zeros before Fourier transformation, and subsequently unbiasing the average autocorrelation sequence. Calculating the average autospectrum of a population, rather than the average autocorrelation, reduces the required number of Inverse Fourier Transforms to one. The necessary assumptions were described for using spectral analysis to form a geometric covariance matrix.

c. A method was shown for separating random and non-random surface variations.

2. A unique method for calculating the variance of assembly stress at every node in a flexible part was developed, which includes covariance effects.

a. Covariance exists between the displacement of all degrees of freedom in the finite element assembly model. This requires that assembly stress variance solutions be solved for every node in the part simultaneously.

b. Kinematic and material properties matrices must be formed which include every degree of freedom in the part. Traditional element-by-element stress

solutions do not account for inter-nodal covariance of stress throughout the part.

3. The FASTA method was verified by comparing predicted assembly results with those predicted by a Monte Carlo simulation. Closure force and assembly stress results were compared, and differences between the results were discussed.
4. FASTA method results were also compared to results from direct statistical calculation of the input gap covariance matrix. This method does not require any assumptions about stationarity of the surface variations, nor does it require performing any FFT's. It does, however, require a large sample size for accuracy.
5. Representing surfaces of flexible parts in the frequency domain provides a method for calculating, specifying, and controlling adequate tolerances on surface variations.
    a. Because variations of different wavelength affect assembly results differently, the sensitivity of assembly deformation, force, or stress to individual wavelengths of surface variation must be determined. The FASTA method can provide these sensitivities, and surface variation tolerances can be determined which are necessary to keep assembly results within acceptable limits.
    b. Tolerances on surface variations of flexible parts can be described by allowable frequency spectra.
    c. Frequency spectrum tolerances can be used to predict expected assembly results before production.

d. Different manufacturing processes cause surface variations of different wavelength. Data can be collected for typical surface variations caused by particular processes. Expected surface variation can be predicted prior to production, based on previous results using similar manufacturing processes.

e. By using spectral analysis to model surface variations, wavelengths of random variation which are causing out-of-tolerance assembly results can be identified, and the sources of those variations can be located and controlled. The FASTA method separates random variations from average, non-random surface variations. Sources of non-random variation, such as part warping, inaccurate tooling, or other non-random process characteristics, can be identified and controlled separately.

6. The wavelength sensitivity of assembly results was demonstrated by predicting interior part stresses due to four different single-wavelength surface variations. Results showed that shorter-wavelength variations produce a larger range of assembly stresses, which are concentrated along the mating edge of the part. However, it is also noted that shorter-wavelength variations typically also have much smaller amplitudes, minimizing their effect on assembly results.

7. The effects of frequency aliasing, leakage, and sample rate were also considered.

   a. The sample rate for measuring surface variations must be fine enough to detect all significant wavelengths of variation.

b. No error is introduced into the assembly model from frequency leakage or aliasing, if the location of finite element nodes corresponds to the location of measured surface variations.

c. Measured surface data can be re-sampled at a lower rate to avoid including a large number of finite element nodes along the mating edge of the assembly model.

8. Contributions were also made to Monte Carlo analysis of flexible assemblies.

a. All statistical analyses of flexible assemblies must account for covariance between nodal variations in the finite element model. Monte Carlo simulation of flexible assemblies must model surface variations as random surfaces rather than sets of random points in order to properly simulate covariance effects due to surface continuity.

b. Monte Carlo analysis of linear flexible assembly models is unnecessary, because it is equivalent to calculating the mean and covariance of surface variations and using them as input into the model. The results are identical if a linear model is used.

c. Monte Carlo simulation requires a large population of surface variations to predict accurate assembly results.

d. Using stiffness matrix condensation and equivalent stiffness matrices can reduce computation time for Monte Carlo simulations.

10.3 Comparison of Methods

Monte Carlo analysis of linear flexible assembly models is unnecessary, because it is equivalent to calculating the mean and covariance of surface variations and using them as input into the model. Monte Carlo analysis requires a large population of surfaces for accurate assembly results, and performs a finite element analysis for each surface. This requires an enormous amount of calculation and run-time. Monte Carlo analysis is useful for predicting statistical results from non-linear models, such as large deformation problems, but is unnecessary for linear flexible assembly statistical analysis.

If a sufficiently large sample of data exists for a population of surface variations, the direct statistical method is the fastest and most accurate method for predicting assembly results using a linear finite element model. A covariant assembly solution is still required, but the direct method calculates the input surface variation covariance matrix directly from the surface data, using the statistical definition. The results are identical to a Monte Carlo analysis of every part in the sample, but with far less computation time. Only two finite element solutions are required, one for the mean and one for the variance or standard deviation. The direct statistical method for forming the covariance matrix is not useful for controlling manufacturing processes, however, because sources of variation cannot be isolated and reduced.

The FASTA method for analyzing flexible assemblies can be used when no data exists for a population, such as in the design stage. If expected surface variations can be assumed to have uniformly random phase, a single frequency spectrum can be used to represent an entire population of parts. The FASTA method also gives more accurate

results than either Monte Carlo or the direct method when surface variation data exists for only a small sample of a population. Averaging of covariance across each surface as well as through the population causes faster convergence to the covariance of the entire population.

The efficiency of the FASTA method is particularly evident in the prediction of assembly stress at interior nodes in a part. Rather than performing an element-by-element solution for every possible assembly and calculating the mean and variance of the stress components at every node, only two solutions are required to predict the statistical distribution of stresses throughout the part.

One additional application of the FASTA method is to locate sources of surface variation which are causing unacceptable assembly results. If frequency spectra of sample part surfaces are examined, wavelengths of variations which are contributing to assembly problems can be located and reduced, bringing assembly results back into an acceptable range. Mean and random variations due to bias and random errors are separated in the FASTA method and are analyzed and can be treated independently.

10.4 Limitations of the FASTA Method

The nodal spacing along mating edges of the finite element assembly model limits the minimum wavelength of surface variation which can be included in the analysis. Variations with wavelength less than twice the nodal spacing must either be excluded from the analysis, or a finer node spacing must be used along the mating edges.

The FASTA method assumes that the covariance of random surface variations is stationary along the mating part surfaces. This assumes that all random surface variations have uniformly-distributed phase, and that the frequency content of the random variations is the same along the entire surface. These assumptions should be accurate for most manufactured part surfaces, but the stationarity of surface variations should be checked for each particular manufacturing process.

The FASTA method predicts the mean and standard deviation of the probability distribution of deformation, closure force, and stress in flexible assemblies. Higher-order moments of the distribution, such as skewness and kurtosis, have not yet been predicted using the spectral analysis technique. Because a linear finite element model is used for the assembly, only skewed surface variation distributions will produce skewed assembly results.

A linear finite element model must be used to represent flexible assemblies in the FASTA method. The model assumes that the gap between every pair of aligning finite element nodes along mating edges is forced to zero when assembled. This assumption is accurate if fasteners are spaced closely together relative to the amplitude of surface variations. Using a linear model allows the FASTA method to calculate the mean and standard deviation of assembly results with only two finite element solutions. Non-linearities in the model, such as contact between fasteners, large deformations, and material yielding, would be difficult to include in a direct statistical analysis.

10.5 Recommendations for Future Work

A new method has been developed and presented for statistical tolerance analysis of flexible assemblies using spectral analysis of surface variations. Future work in this area should expand and further verify the new method.

The FASTA method has been presented and verified in this paper using an example flexible assembly involving line contact along a common mating edge. Future work should apply the method to joints involving surface contact between parts. Covariance would exist between degrees of freedom at all finite element nodes in the contacting region. The geometric covariance would need to be defined for surface variations in the entire area. If the covariance is stationary for the entire surface, the same autocorrelation function could be used to form the covariance matrix for the whole region. Otherwise, another method must be used to define the covariance between all degrees of freedom involved in the mating surface.

Simple two-dimensional plates were used in the example assemblies demonstrating the FASTA method. Future work could apply the method to three-dimensional flexible parts. If the parts are thin, three-dimensional plate and shell finite elements could be used to model their flexibility. The procedure for analysis would be the same, but six global degrees of freedom would exist at each node. Surface variations could exist in more than one global coordinate direction.

A method for finding explicit relationships between surface variation frequency spectra and assembly results should be developed. These relationships are needed in tolerance allocation for flexible assemblies. If the linear finite element assembly model is

viewed as a transfer function, a frequency response function could perhaps be used to describe the sensitivity between input surface variation autospectra and the autospectra of output assembly results such as deflection, force, and stress. These autospectra are related to the covariance matrix and therefore to the standard deviation of assembly results. The allowable autospectrum of an assembly result would need to be defined to calculate the allowable surface variation spectrum.

This paper does not address the issue of how deformations occurring at one joint in a flexible assembly affect other mating surfaces. Deformations due to joining two flexible parts will propagate through the assembly, possibly affecting stress and deformation at other joints. Prediction of these affects would be relatively straightforward, however, as the statistical part displacements predicted using the FASTA method could be superimposed on surface variations from manufacturing along a mating edge or surface. The total displacements in the mating region would be used as input for analysis of that joint in the assembly.

The FASTA method may be used to study the effect of fixtured assembly processes on assemblies of flexible parts having surface variations. Also, the effect that order of assembly has on an assembly of flexible parts could be studied. Work in these areas has been begun by Hu, but does not include the effect of surface variations (Liu 1995, 1997). In a linear model, assembly results from fastening parts in free space and from fastening parts while fixtured and then releasing the assembly are the same. A non-linear or iterative analysis would be required. To study the effect of order of assembly,

the combined stiffness of two or more joined parts must be modeled when they are fastened to another part in the assembly.

Further research should compare predicted assembly results from linear contact models, such as that used in the FASTA method, with those predicted by an iterative solution which includes contact at nodes between fasteners. A method for performing a statistical analysis on non-linear contact models, avoiding a part-by-part simulation, may be developed.

An important area for future research is to compare the results predicted by the FASTA method with results measured from physical assemblies of flexible parts. If a sufficient population of flexible parts are assembled, the statistical distribution of their surface variations and of the assembly results could be estimated. The distribution of assembly results could be compared with the mean and standard deviation predicted by the FASTA method. Assembly strains may be measured by strain gauges attached at the same location on every assembly. Or, the deflections of the parts when assembled could be measured using a coordinate measuring machine.

Eventually, the FASTA method should be integrated into user-interfaced software for statistical tolerance analysis of flexible assemblies. The software could link to existing commercial finite element codes to model the flexible parts if access is granted to internal stiffness and constitutive matrices. Otherwise, the software must include its own finite element solver. A simple method for describing the autospectrum of surface variations, or surface variation data, would need to be developed. Also, the predicted distribution of assembly results would need to be depicted clearly.

REFERENCES

American Society of Mechanical Engineers (1993). "Mathematical Definition of Dimensioning and Tolerancing Principles." *ASME Codes and Standards*, Y14.5.1M-199x.

Anderson, T. (1997). *Surface Variation and Mating Surface Rotational Error in Assemblies*. Master's thesis, Brigham Young University, Provo, Utah.

Bendat, J. and A. Piersol (1986). *Random Data: Analysis and Measurement Procedures*, 2nd ed. John Wiley & Sons, New York.

Francavilla, A. and O. Zienkiewicz (1975). "A Note On Numerical Computation of Elastic Contact Problems." *Intl. Journal for Numerical Methods in Engineering*, v9 p913-924.

Gordis, J. and W. Flannelly (1994). "Analysis of Stress Due to Fastener Tolerance in Assembled Components." *AIAA Journal*, v32 n12 p2440-2446.

Johnson, R. and D. Wichern (1988). *Applied Multivariate Statistical Analysis*, 2nd ed. Prentice Hall, Englewood Cliffs, New Jersey.

Kwon, Y. and H. Bang (1997). *The Finite Element Method using MATLAB*, CRC Press, Boca Raton, Florida.

Liu, S. and S. Hu (1995). "An Offset Finite Element Model and Its Applications In Predicting Sheet Metal Assembly Variation." *Intl. Journal of Machine Tools and Manufacture*, v35 n11 p1545.

Liu, S. and S. Hu (1997). "Variation Simulation For Deformable Sheet Metal Assemblies Using Finite Element Methods." *Journal of Manufacturing Science and Engineering, Transactions of the ASME*, v119 n3 p368-374.

Merkley, K. (1996). "An Introduction to Tolerance Analysis of Flexible Assemblies." *1996 MSC World Users' Conference*, MacNeal-Schwendler Corp., Newport Beach, California.

Merkley, K. (1998). *Tolerance Analysis of Compliant Assemblies*. Ph.D. thesis, Brigham Young University, Provo, Utah.

Stout, J. Unpublished Master's thesis, Brigham Young University, Provo, Utah.

Thomas, T.R. (1982). *Rough Surfaces*. Longman Group Limited, Longman House, U.K.

Thornhill, R. and C. Smith (1994). *Fourier and Spectral Analysis in Dynamic Systems*. The University of Texas, Austin, Texas.